

Supplement for “Effects of mountains and ice sheets on ocean circulation”

OSUVic: The Oregon State University - University of Victoria Earth Climate System Model

Version 0.3

Documentation and Evaluation

Andreas Schmittner¹ and Tiago Silva²

College of Oceanic and Atmospheric Sciences, Oregon State University, Corvallis OR, USA.

¹ aschmitt@coas.oregonstate.edu

² now at University of East Anglia, UK.

11/24/10

Introduction

OSUVic consists of the UVic [Weaver *et al.*, 2001] model (ocean physics, ecosystem and biogeochemistry, sea ice, land surface) coupled to the simplified atmospheric general circulation model Planet Simulator [Fraedrich *et al.*, 2005a; Fraedrich *et al.*, 2005b] via the OASIS coupler. The individual component models and the coupler have extensive histories and documentation. We refer to the web sites (<http://climate.uvic.ca/>, <http://www.mi.uni-hamburg.de/6.0.html>, http://www.prism.enes.org/PAEs/coupling_IO/software_OASIS3.php) for further information. Here, only information pertinent to the coupling and the coupled model performance is described. Additional information and publications are available at <http://mgg.coas.oregonstate.edu/~andreas/OSUVic/>.

Coupling

A total of 14 fields (Figure 1) are exchanged between the models at each coupling timestep Δt_{CPIL} . Precipitation (P), specific humidity (q_{2m}) and air temperature (T_{2m}) at 2 m, meridional and zonal wind stress components (τ_x , τ_y), wind speed ($|u|$), and the downward components of the surface shortwave (F^{SWd}) and longwave radiation (F^{LWd}) are passed from PlaSim to UVic (blue arrows). Surface temperature (T_{sfc}), roughness length (z_0), sensible heat flux (F^{SH}) and evaporation (E), surface albedo (a_{sfc}) and the upward component of the surface longwave radiation (F^{LWu}) are passed from UVic to PlaSim (red arrows). Conservative remapping is used for the fluxes from UVic to PlaSim (E , F^{SH} , F^{SWu} , F^{LWu}) and for the fluxes from PlaSim to UVic (P , τ_x , τ_y , F^{SWd} , F^{LWd}) [Jones, 1999]. For those variables that do not need to be conserved bilinear interpolation is used (T_{2m} , q_{2m} , $|u|$, T_{sfc} , z_0).

Calculation of P , τ_x , τ_y , F^{SWd} , F^{LWd} is according to the PlaSim schemes [Lunkeit *et al.*, 2007] and E , F^{SH} , F^{SWu} , F^{LWu} are calculated using UVic's formulas [Weaver *et al.*, 2001]. It might be desirable in the future to update the calculation of the fluxes in UVic with the PlaSim boundary layer scheme, which considers stratification.

At the end of the shortwave routine in PlaSim the upcoming shortwave radiation at the surface $F^{\uparrow SW}$ is replaced by the UVic flux. The surface albedo is diagnosed according to $R_S = F^{\uparrow SW} / F^{\downarrow SW}$ and used in the subsequent call to the radiation scheme. The longwave flux emitted from the surface $A_S B(T_S)$ (see equation 3.56 in Plasim Manual) is replaced by the UVic flux. The surface emissivity is diagnosed according to $A_S = F_{UVic}^{\uparrow LW} / B(T_S)$ and then used to calculate the reflected component of the up going longwave radiation $(1 - A_S) F_{L+1}^{\downarrow LW}$.

The time stepping scheme is shown in Figure 2. Different time steps are used. The atmospheric time step is the shortest. At T21 resolution $\Delta t_A = 45$ min, and at T42 resolution $\Delta t_A = 20$ min is used. The sea ice and land surface models use a time step of $\Delta t_{IL} = 7.5$ h and the ocean model uses a time step of $\Delta t_O = 30$ h for the advection of tracers. Fluxes are exchanged between the atmosphere and the sea ice/land surface every two land/ice time steps $\Delta t_{CpIL} = 2 \times \Delta t_{IL} = 15$ h (T21). Fluxes between the ocean and the sea ice and atmosphere are exchanged every $\Delta t_{CpO} = 2 \times \Delta t_O = 60$ h = 2.5 d.

Currently three CPUs are used, one for PlaSim, one for OASIS and one for UVic. During each ocean coupling time step Δt_{CpO} the following sequence is used (see Figure 3). (1) Initially the atmosphere and the ocean models run parallel. (2) Fields are passed - either directly from the ocean or via OASIS from the atmosphere - to the surface (land/ice) model. (3) The surface model integrates two time steps, during which the ocean and atmosphere models wait for input. (4) Information is passed to the atmosphere. (5) The atmosphere is stepped forward for $\Delta t_{CpIL} / \Delta t_A$ time steps. (6) Fields are passed from the atmosphere to the surface model. (7) The surface model runs two time steps and (8) passes information to atmosphere and ocean.

Changes to Original Model Code and Setup

PlaSim. Initial test runs showed that the default PlaSim parameter setting leads to a too cold climate (global SST=288 K, or 3 K colder than observed), too high planetary albedo (35.7% versus 28-34% estimated from observations [Trenberth *et al.*, 2009]) and too little global cloud cover (55% versus 62% estimated from ISCCP satellite observations). Therefore some PlaSim parameter values have been adjusted from their default setting. In particular the cloud albedo has been decreased (TSWR1=0.033(0.26 in T42), TSWR2=0.033, TSWR3=0.06) from the default setting (TSWR1=0.04, TSWR2=0.048 TSWR3=0.004) and the critical humidity for cloud formation has been set to decrease from 0.82 at the surface to 0.72 at the TOA (the PlaSim default value was 0.85 and higher at the top and bottom levels). (Variables TSWR1-3 in the code correspond to f_{b1}, f_{b2} and f_{o2} in equations 3.31 to 3.42 of the Plasim version 15.0 reference manual). These changes lead to global mean SSTs and cloud cover close to observations.

As will be discussed in more detail below all model versions have a strong cold winter bias in the Arctic. This bias could be slightly improved by changes to the long wave radiation code. Temperature dependency of transmissivities for water vapor, CO₂ and ozone is now taken into account according to Sasamori [1968] using the temperature averaged along the path and weighted by the absorber amount. This increased absorption and emission of longwave radiation. The global downward longwave flux at the surface (344 W/m²) is now near the upper end of observational estimates (324-345 W/m²).

UVic. We use UVic version 2.8 with parameter setting as described in [*Schmittner et al., 2008*].

Comparison with Observations

The figures below show runs of model version 0.3.1. In this model version vegetation on land is fixed. (Coupling the dynamic vegetation model TROLL is currently in progress). The T42 version has been run for more than 500 years, the T21 version for more than 700 years. Most figures presented below use an average of model years 750-760 (T21) and 660-669 (T42). The deep ocean is still experiencing drift in the T21 version but the T42 version is in a statistical equilibrium state (Figure 4). The surface in T21 is close to a statistically steady state. A considerable imbalance (-2 to -3 W/m²) remains at the top of the atmosphere (TOA) in both model versions. A similar imbalance is found in the PlaSim stand-alone version.

In the tropics incoming solar radiation is 10-20 W/m² to small, whereas it is overestimated at mid and high latitudes (Figure 6, Figure 7), whereas the outgoing longwave radiation is in good agreement with observations. The net energy gain at low latitudes and the net energy loss at high latitudes is therefore underestimated in the model, which is also the case for the meridional energy transport. The planetary albedo is too large over the low latitude oceans (Figure 8), whereas it is too small over land and at mid latitudes between 40-70°N/S over the oceans.

The surface albedo is in good agreement with observations over sea ice-free (<60°N/S) oceans (Figure 10). However, over high latitude land surfaces in the northern hemisphere between 50-70°N the surface albedo is too low, whereas it is too high over eastern central Asia between 30-45°N, explaining the biases in the planetary albedo there.

The planetary scale features of global cloud distribution as estimated from satellites are reproduced by the model, such as large cloud cover (> 70%) over the mid-latitude oceans and along the Intertropical Convergence Zone (ITCZ), and little cloud cover in the subtropics, particularly over land (Figure 12). However, cloud cover is too large over equatorial regions of the central and eastern Pacific, the Atlantic, and the western Indian ocean along the east coast of Africa, explaining the overestimated planetary albedo there. Cloud cover is underestimated over large areas of the extratropical ocean. Interestingly cloud cover is generally less in the higher resolution model (Figure 13, Table 1).

	Cloud Cover (%)	Planetary Albedo (%)	Surface Albedo (%)	Precip (mm/d)	Evap (m/a)	Runoff (10^3 km 3 /a)
Obs	62	28-34	14-28 most 15	2.6	1.1	40
T21	65	34	20	3.1	1.1	36.7
T42	60	32	20	3.1	1.1	33.6

	STRD (W/m 2)	STR (W/m 2)	SSW (W/m 2)	SSH (W/m 2)	SAT (C)	SST (K)
Obs	324-345	48-73	156-169	15-24		291
T21	346	48	159	22	14.6	291.5
T42	346	51	168	26	14.9	291.6

Table 1: Global averages of top-of-the-atmosphere and surface properties and fluxes in comparison to observation based estimates [Trenberth et al., 2009].

Abbreviations: STRD=Surface Thermal Radiation Downward, STR=Net Surface Thermal Radiation, SSW=Surface Shortwave, SSH=Surface Sensible Heat Flux, SAT=Surface Air Temperature, SST=Sea Surface Temperature. Model results were averaged over model years 750-759 (T21) and 660-669 (T42).

Zonally averaged air temperature is generally well simulated, except a warm bias in the low latitude stratosphere and cold biases in the Arctic at low and high altitudes (Figure 14-Figure 15). Specific humidity, however, shows a systematic dry bias at \sim 800 hPa in the atmosphere Figure 16.

The zonally averaged circulation (Figure 18 - Figure 21) is broadly consistent with observation-based estimates [Peixoto and Oort, 1992] and the NCAR/NCEP reanalysis, showing an upper level zonal jet, which is stronger in the winter hemisphere than in the summer hemisphere, and a Hadley circulation of $15\text{-}20 \cdot 10^{10}$ kg/s seasonal overturning. The Hadley cell is 10-20% stronger in the higher resolution model compared to the lower resolution model. In the southern hemisphere the westerly wind jet in the low resolution model is too narrow, does not extend far enough south and far enough towards the surface compared with the NCAR/NCEP reanalysis. This leads to too weak surface westerly wind velocities with the maximum displaced northward. At T42 resolution the upper level width of the westerly wind jet and its southward and downward extension is much better captured.

Surface air temperatures display a strong cold bias over the Arctic (Figure 22-Figure 23), particularly in winter (Figure 24) and more so in the low-resolution model version. North of 70° the air is more than 15°C too cold, with most of the bias located over the Atlantic/Eurasian sector of the Arctic. Over land surface temperatures are too warm, particularly in summer, whereas over the ocean they are too cold, particularly in the subtropics. The cold bias over the subtropical oceans in the northern hemisphere appears stronger in summer than in winter.

Surface specific humidity is too low over land, despite warmer air temperatures. This implies that the surface air relative humidity is much too low. This dry bias over land is

presumably leading to too low soil moisture with attendant problems for the simulation of dynamic vegetation.

Precipitation is in reasonable agreement with satellite-based estimates in both models, with the exception of a wet bias over the eastern subtropical ocean basins (Figure 32). T42 has a double ITCZ. Precipitation over the West Pacific Warm Pool is underestimated, suggesting a too weak Walker circulation. The model reproduces seasonal variations in precipitation associated with the Austral-Asian and African monsoon systems. At T42 resolution a pronounced double ITCZ is simulated in both seasons, in contrast to observations.

Zonal wind stress over the ocean is much better in T42 than in T21 (Figure 38). Particularly over the Southern Ocean wind stress is much too weak in T21 and the maximum of the westerlies is much too far north. This leads to too little Ekman divergence and underestimated upwelling. These biases are typical for coarse resolution atmosphere models [*Farneti and Vallis*, 2009].

The surface westerly wind bias in the T21 model version forces an Antarctic Circumpolar Current (ACC) much weaker (30 Sv) than observed (130 Sv), whereas in the T42 model version the ACC is in much better simulated (100 Sv). The meridional overturning circulation in the Atlantic (AMOC, Figure 42) is much too weak (6 Sv) and too shallow in T21 (Figure 43), whereas it is well simulated in T42 (12 Sv) (Figure 44). This large sensitivity of the mean state of the AMOC to the atmospheric model resolution is interesting and consistent with results from the NCAR model [*Bryan et al.*, 2006]. A sensitivity experiment at T21 resolution with prescribed NCEP wind stress reveals that the AMOC is not very sensitive to the wind stress (not shown). The T21 model version has almost no Antarctic Bottom Water (AABW) formation and considerably less inflow of AABW and Circumpolar Deep Water into the Atlantic, Indian and Pacific ocean basins.

Sea surface temperatures exhibit an overly zonal structure in the model with too warm waters in eastern equatorial upwelling regions of the Pacific and Atlantic oceans. The subtropical gyres are too cold, particularly in the northern hemisphere, whereas the warm pool in the western equatorial Pacific is meridionally too narrow and does not extend far enough northward (Figure 45). The subpolar North Atlantic is too cold in the T21 model version owing to the underestimated meridional heat transport by the AMOC, whereas in the T42 model version the cold bias is restricted to the Nordic Seas and temperatures south of Iceland are in good agreement with observations.

The surface net shortwave radiation is overestimated over land and underestimated over the oceans such that the zonal mean is in good agreement with observations (Figure 47, Figure 48). This biased land sea distribution of the shortwave radiation is likely the main explanation for the too warm land surface and the too cold oceans (Figure 22).

The simulated distribution of downwelling longwave radiation, with low values over dry subtropical land areas and high values over the oceans, agrees well with the ERA40

reanalysis, but OSUVic overestimates back-radiation in the tropics and underestimates it in the Arctic, over the northern hemisphere oceans and over Siberia. Net longwave cooling is generally too small over ocean surfaces (Figure 51) and too large over some land areas such as the Near- and Mideast and Antarctica. Those biases seem to be somewhat smaller in the T42 model version. Biases in the sensible heat flux (Figure 53) are generally small over the oceans but overestimated over land.

Figures

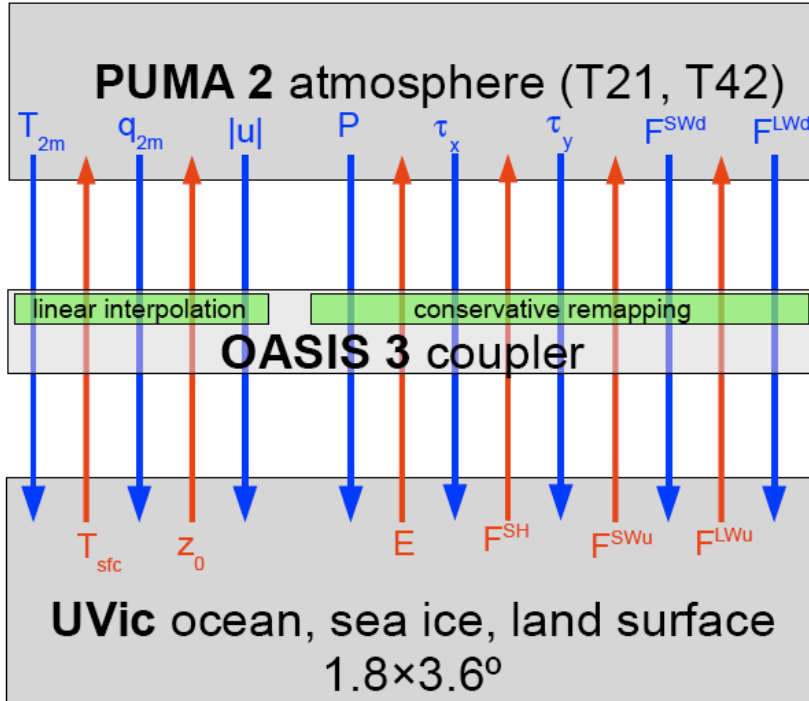


Figure 1: Fields exchanged between the UVic model and PlaSim. The OASIS (version 3) coupler is used for conservative remapping of surface fluxes between the different model grids. Other variables that are required in one model from the other model, e.g. in the calculation of surface fluxes or for the convection scheme, are linearly interpolated between the model grids.

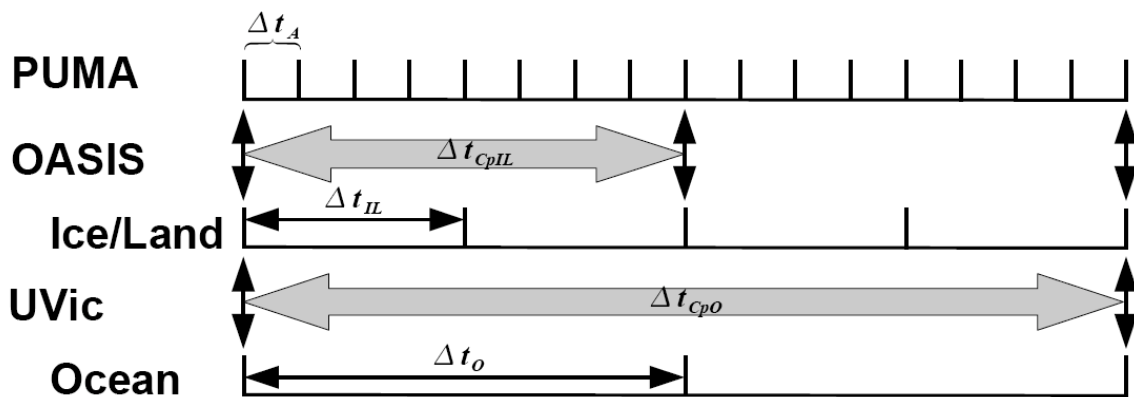


Figure 2: Time stepping of the coupled model.

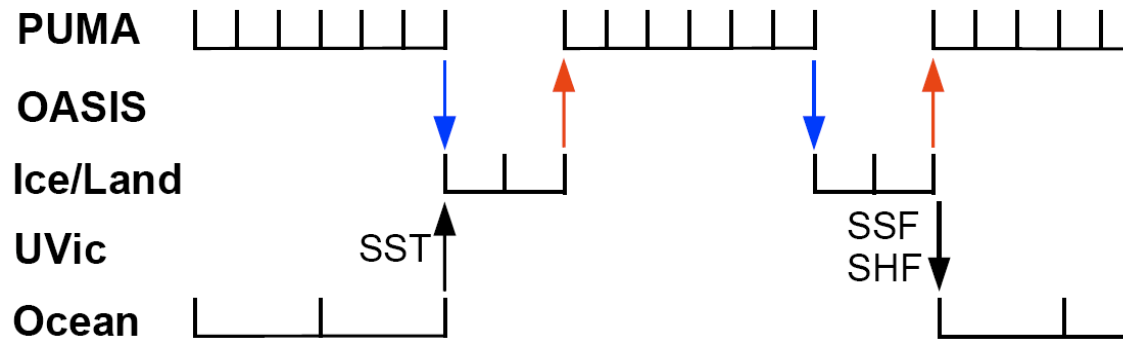


Figure 3: Coupling sequence. Each ocean coupling time step the ocean passes SST to the ice and receives surface salt flux (SSF), surface heat flux (SHF) and momentum fluxes (wind stress). The red and blue arrows correspond to those of Figure 1.

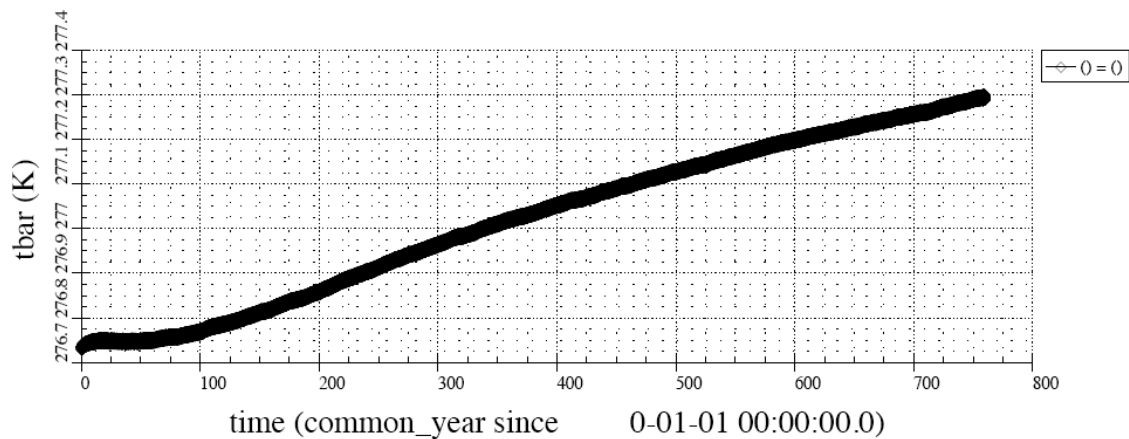
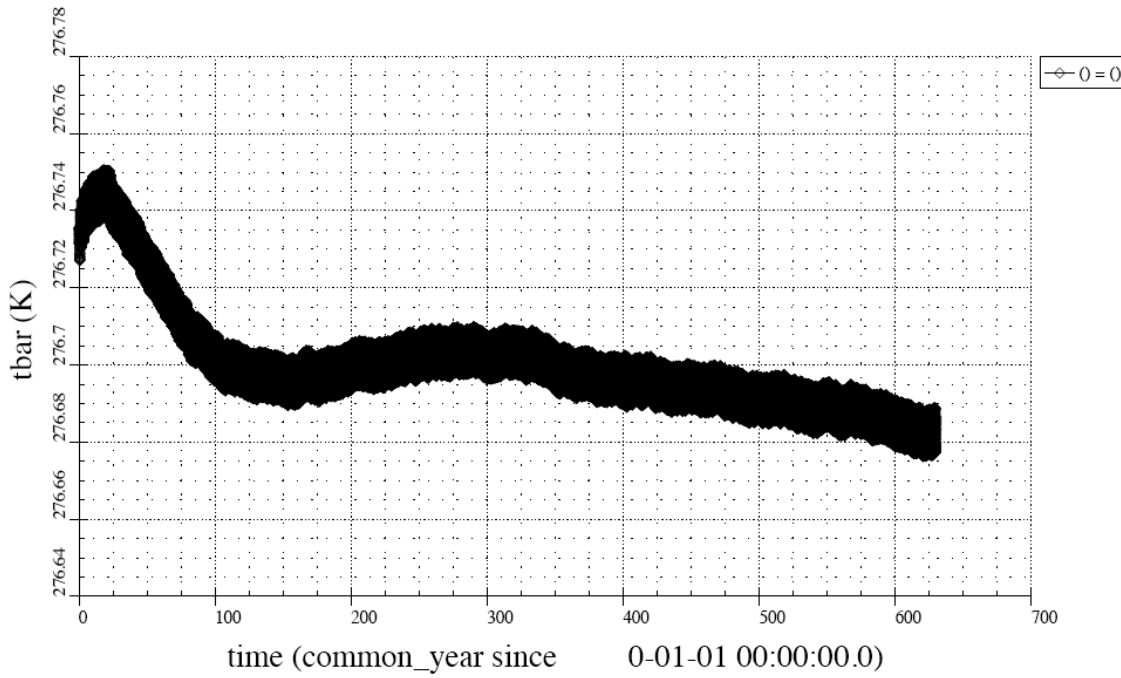


Figure 4: T21 Global average ocean temperature.



Global average T

Figure 5: T42 Global average ocean temperature.

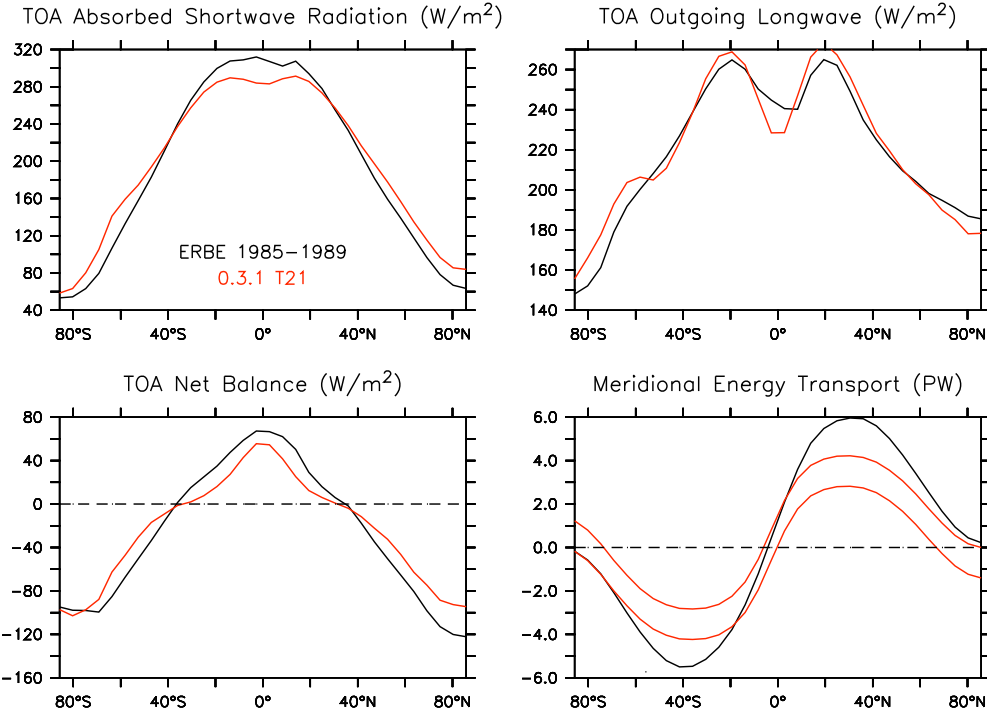


Figure 6: T21 TOA fluxes. The meridional heat flux was calculated by integration of the TOA net flux. Upper line starts from north pole, lower line from south pole. Difference is due to global imbalance (=error).

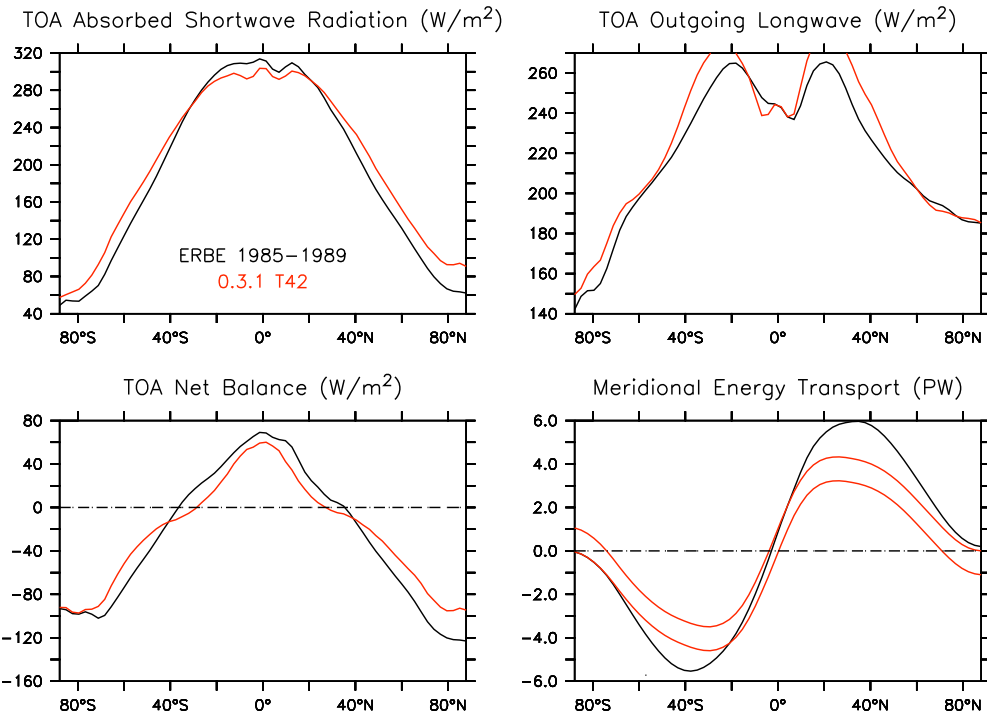


Figure 7: T42 TOA fluxes.

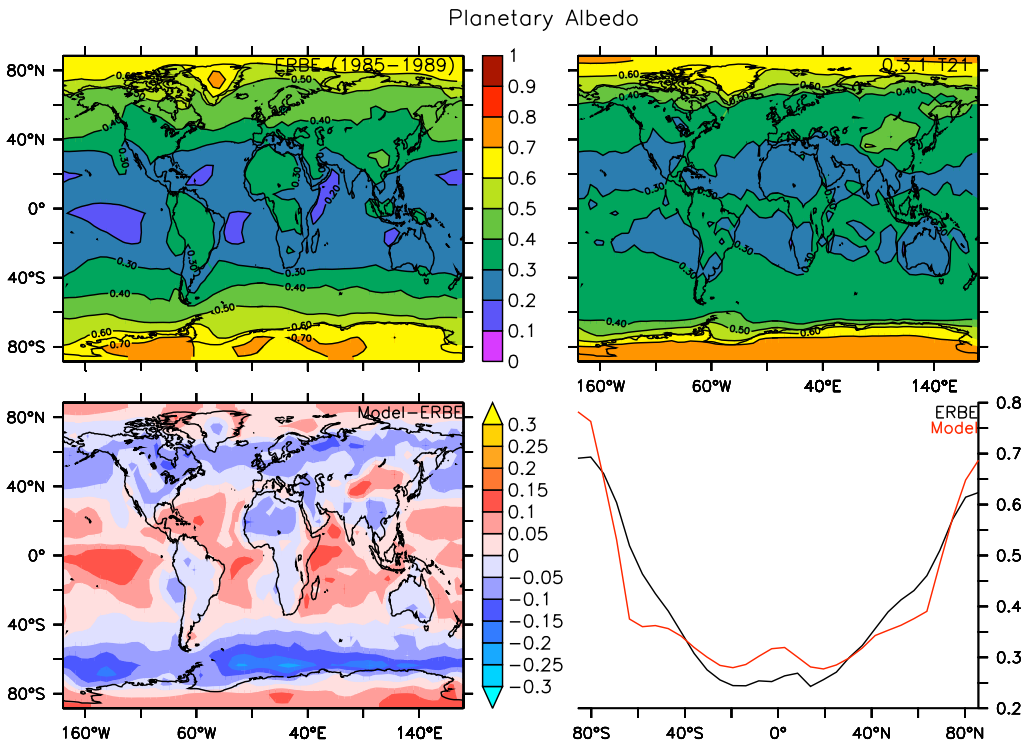


Figure 8: T21 Planetary albedo.

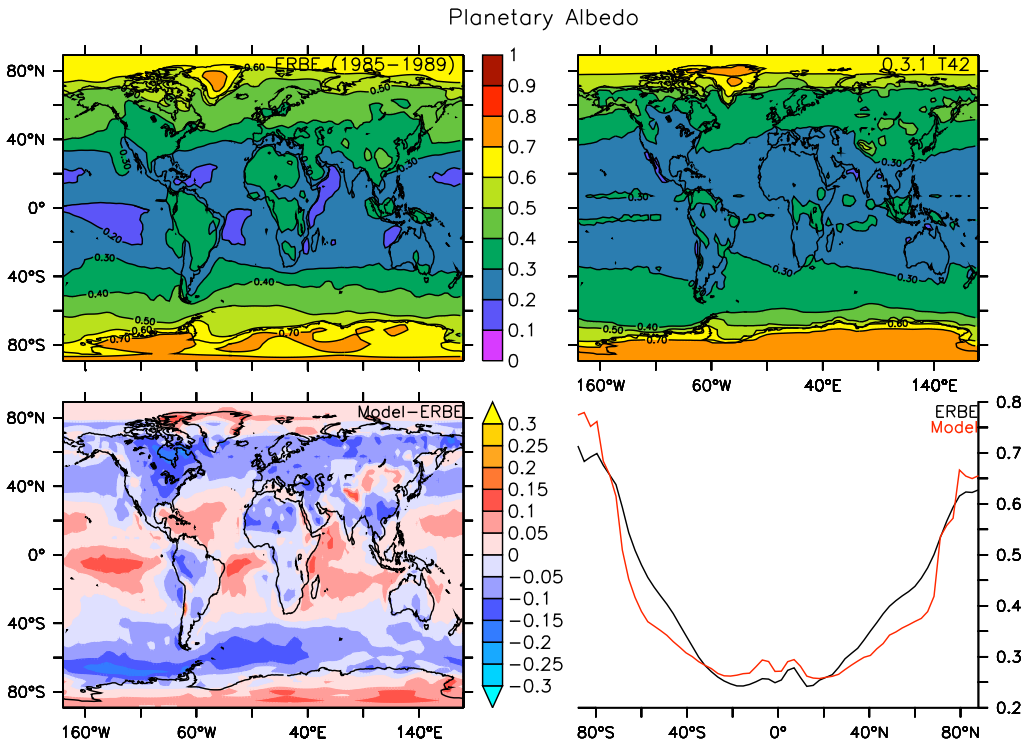


Figure 9: T42

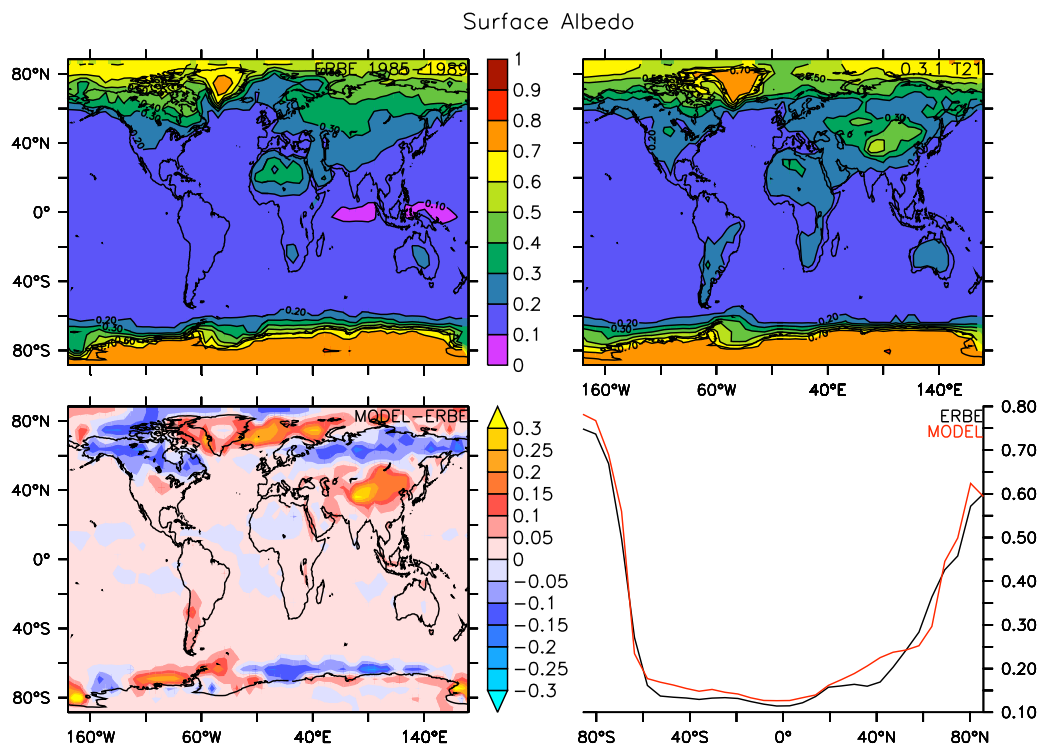


Figure 10: T21 Surface albedo.

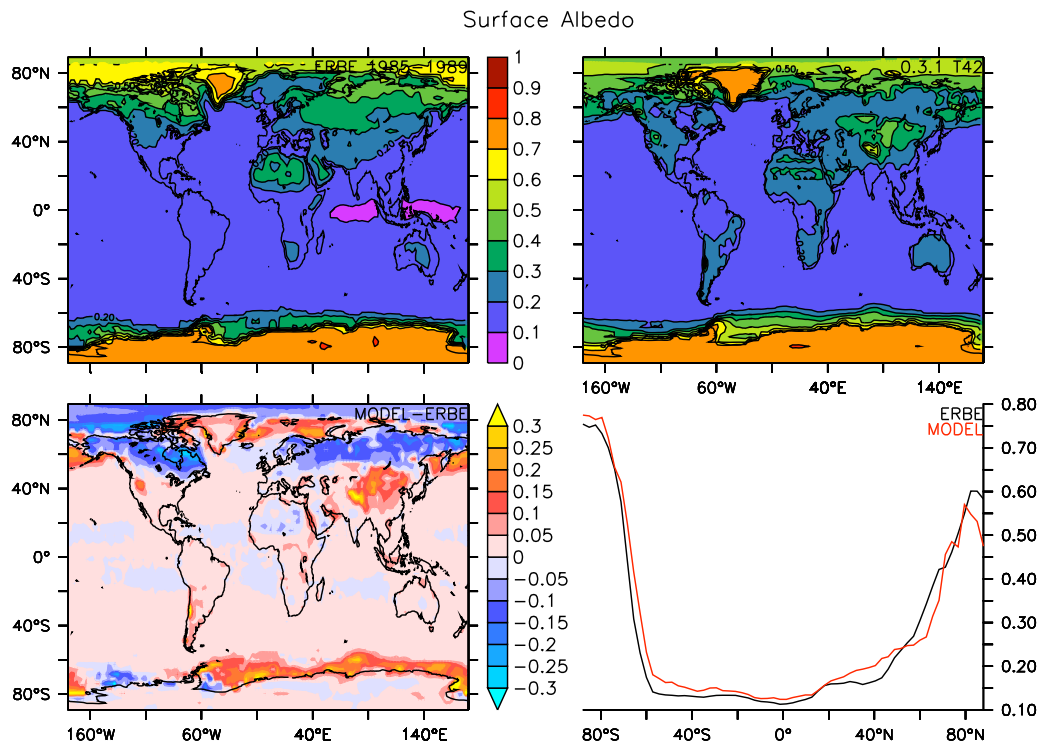


Figure 11: T42

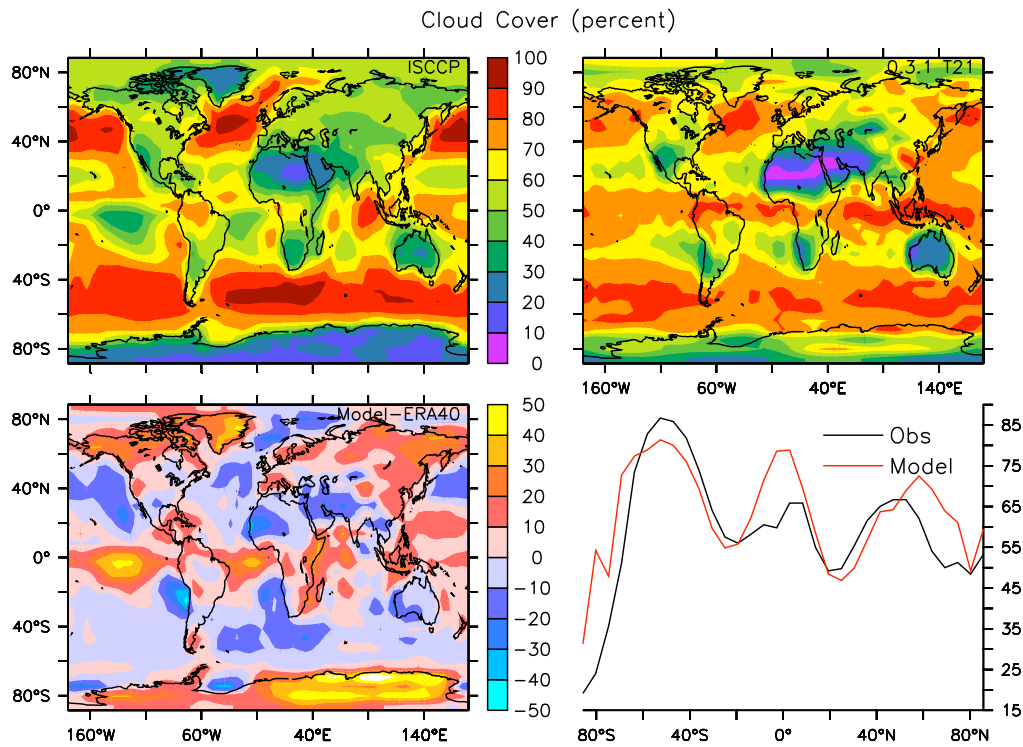


Figure 12: T21 Cloud Cover.

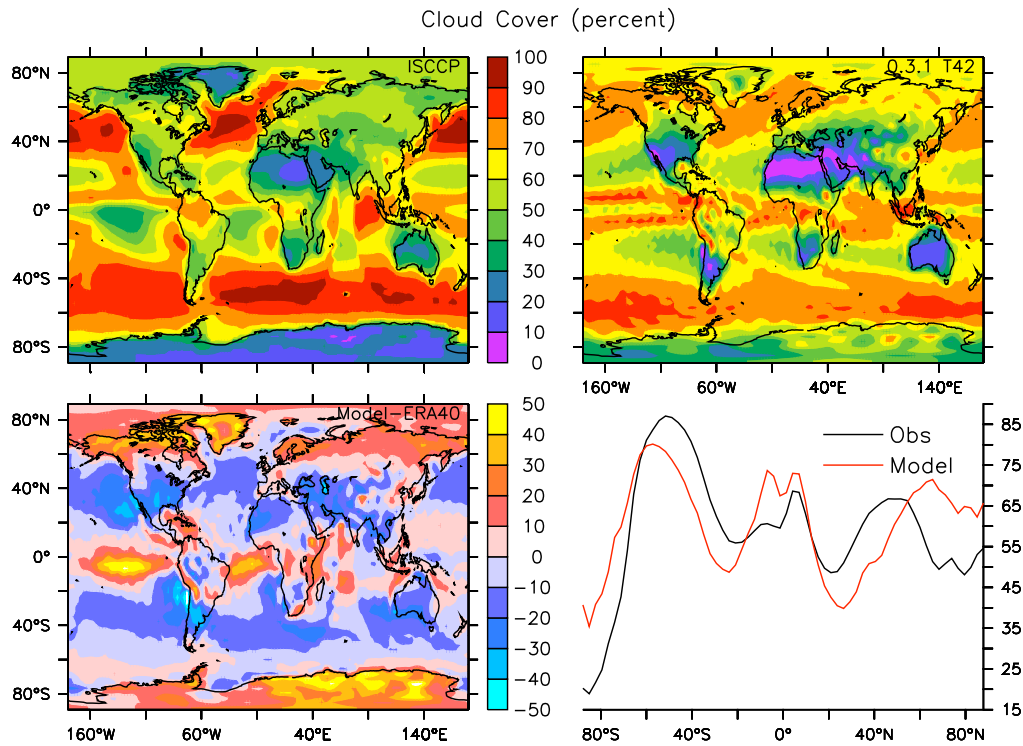


Figure 13:

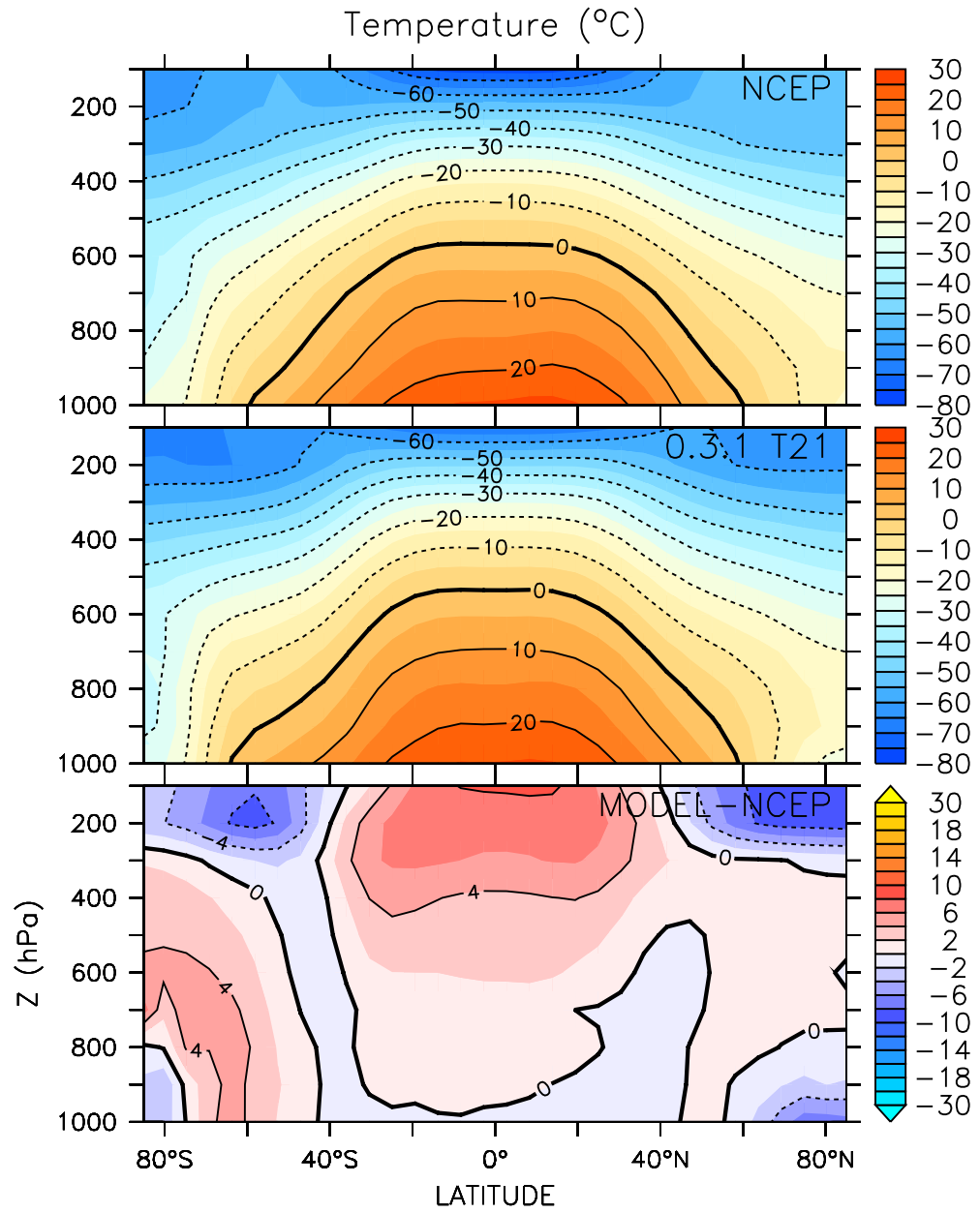


Figure 14: T21 Zonally averaged air temperature.

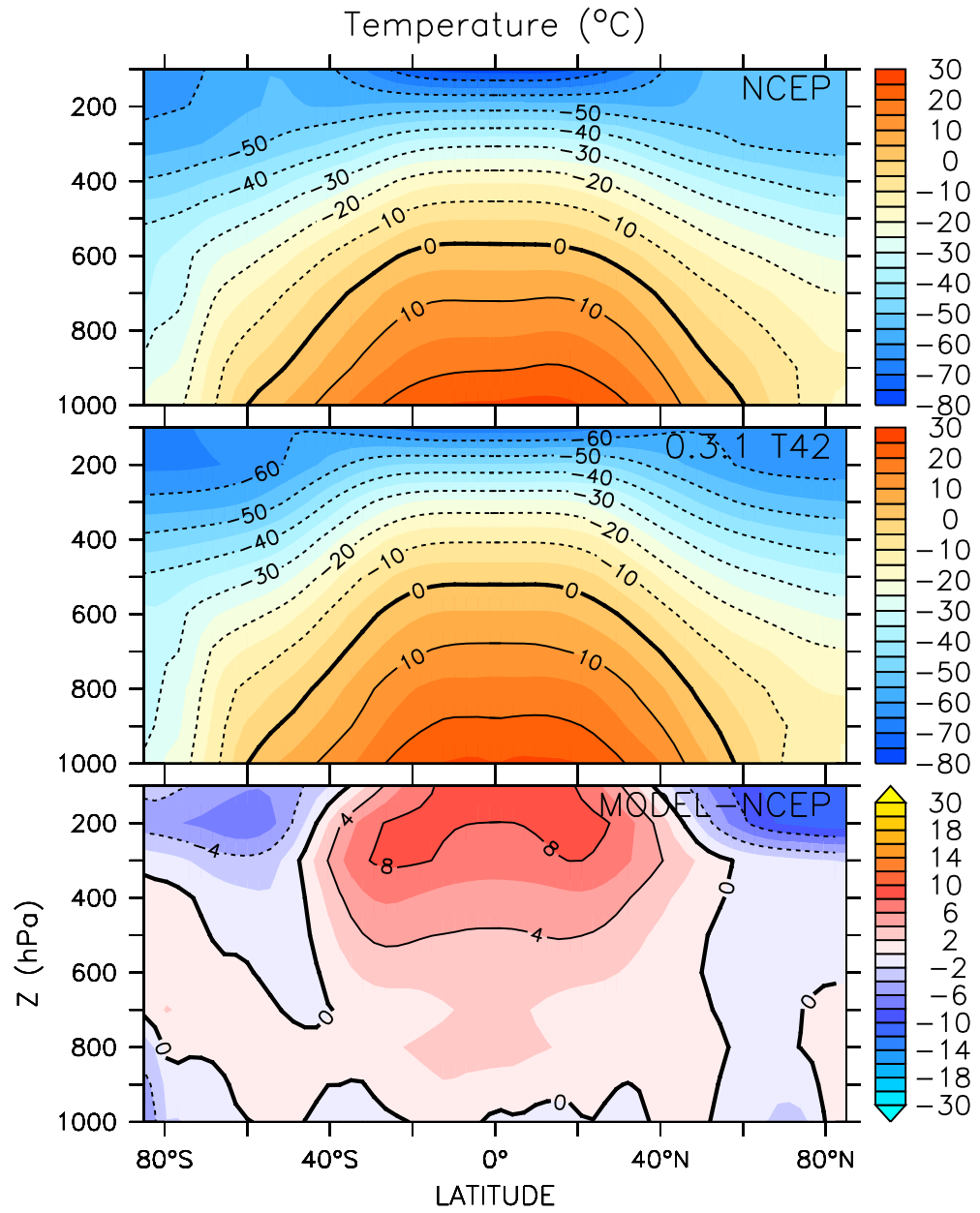


Figure 15: T42

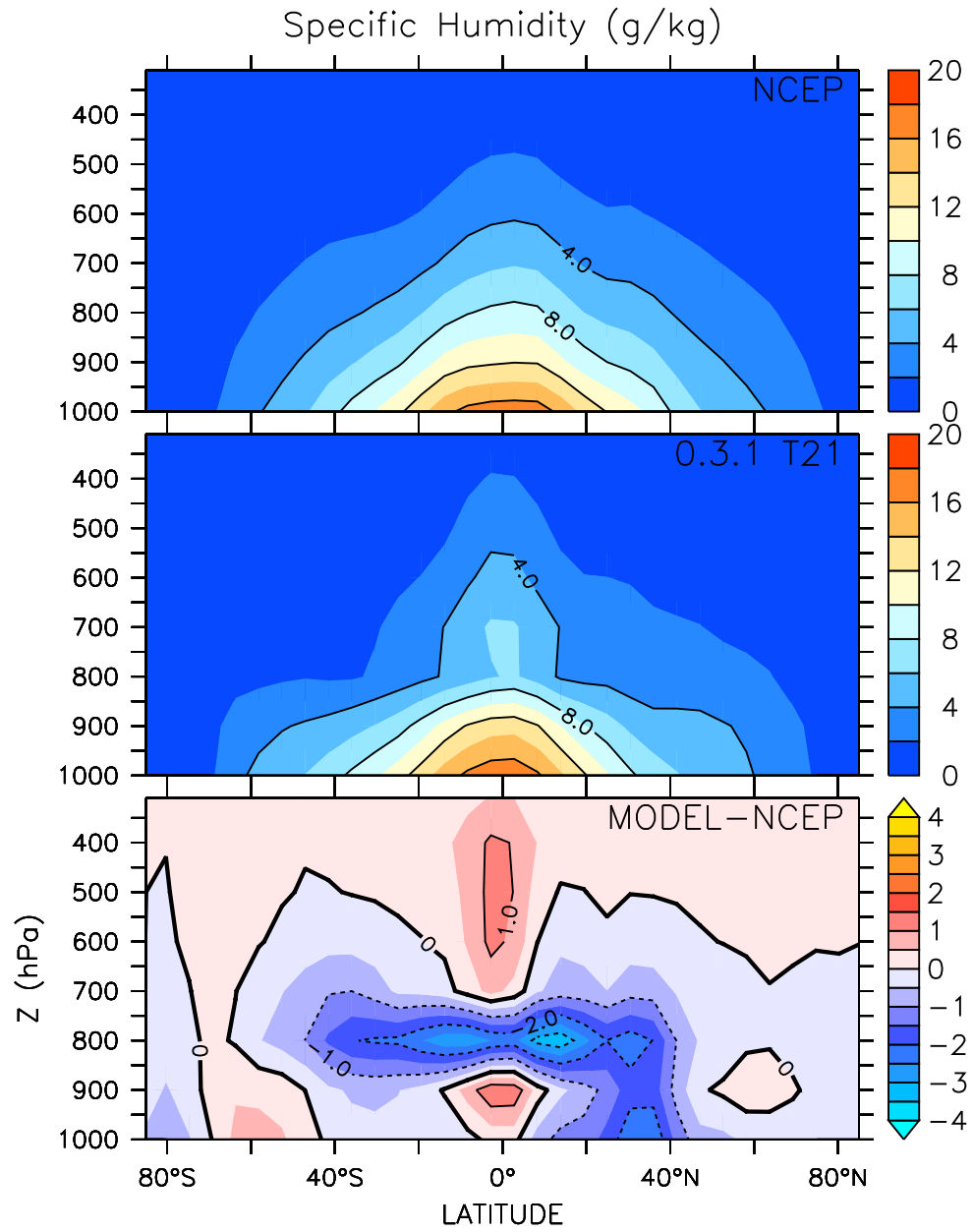


Figure 16. T21 Zonally averaged specific humidity.

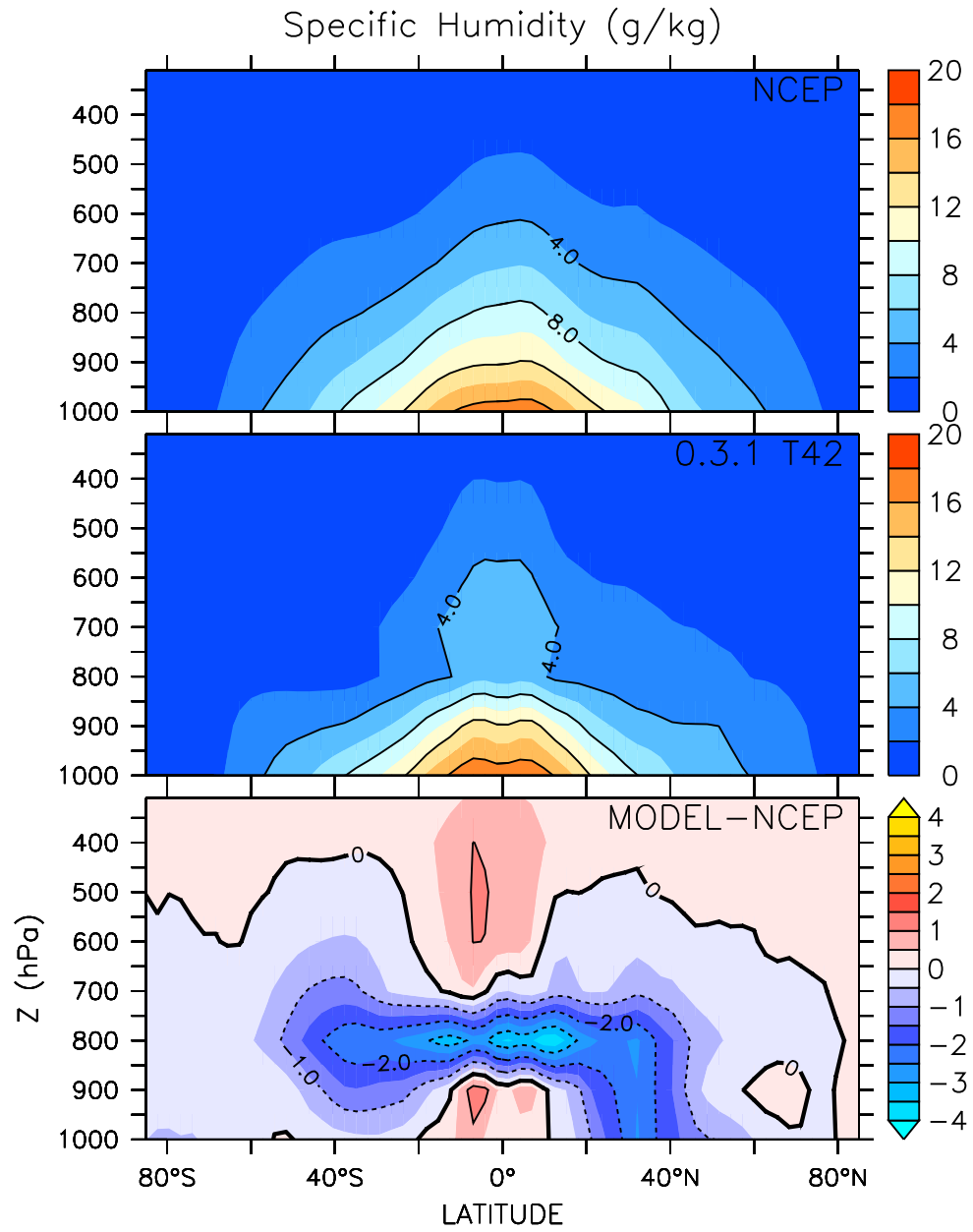


Figure 17. T42 Zonally averaged specific humidity.

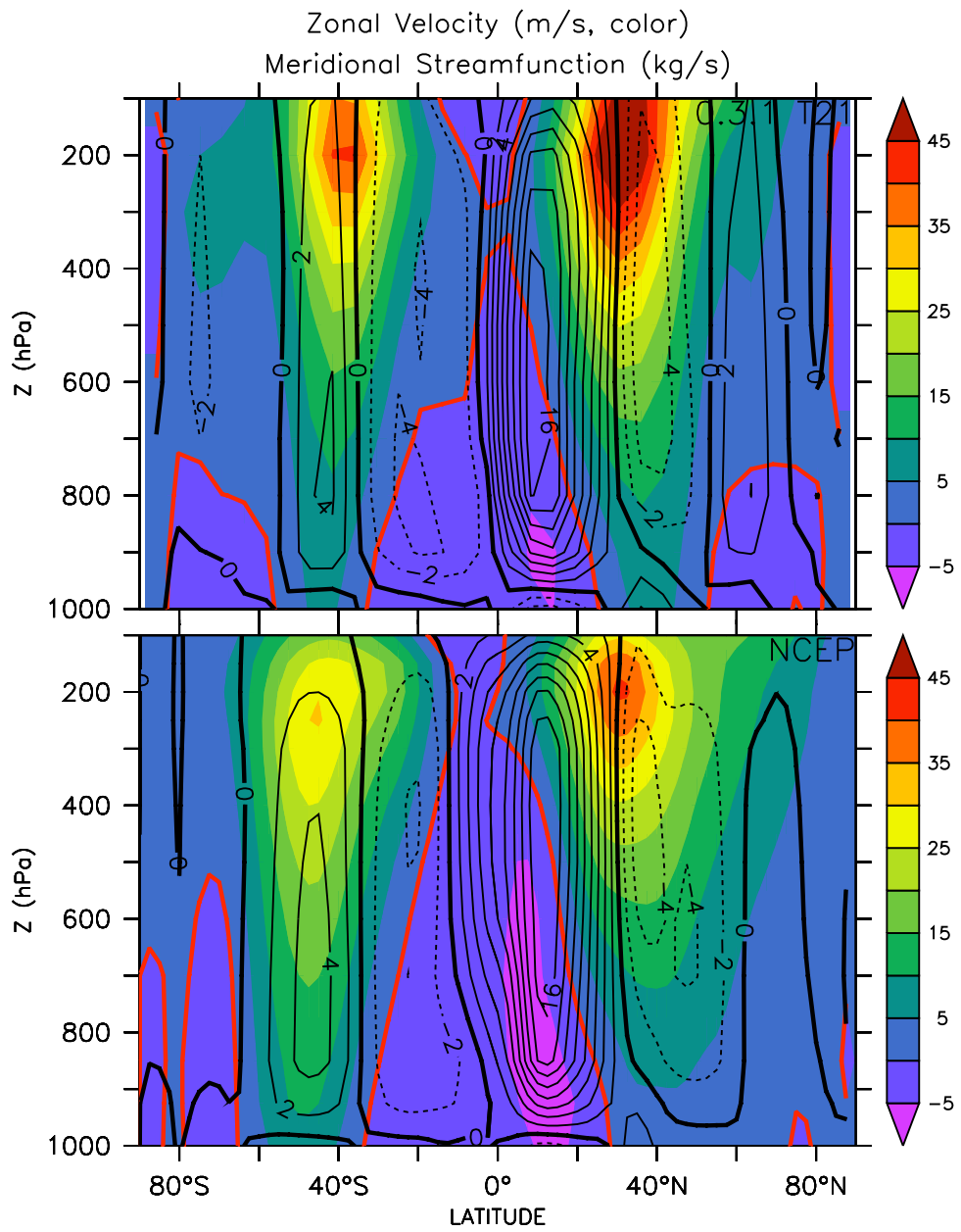


Figure 18: T21 Atmospheric Circulation DJF: Zonal mean zonal wind (color, zero contour line in red) and meridional mass streamfunction (black contour lines). Positive (negative) values correspond to solid (dashed) lines and clockwise (counter clockwise) flow direction.

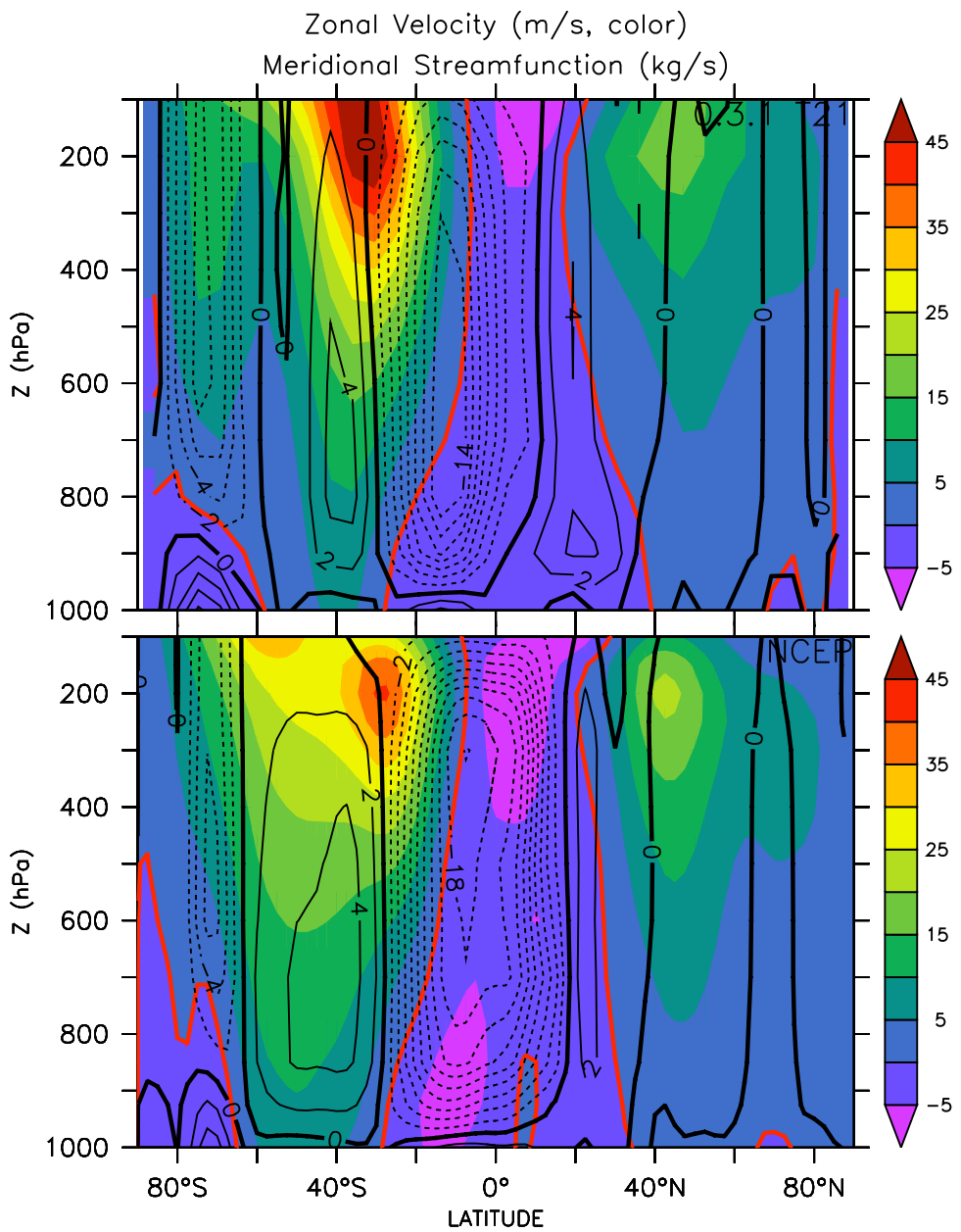


Figure 19: T21 JJA

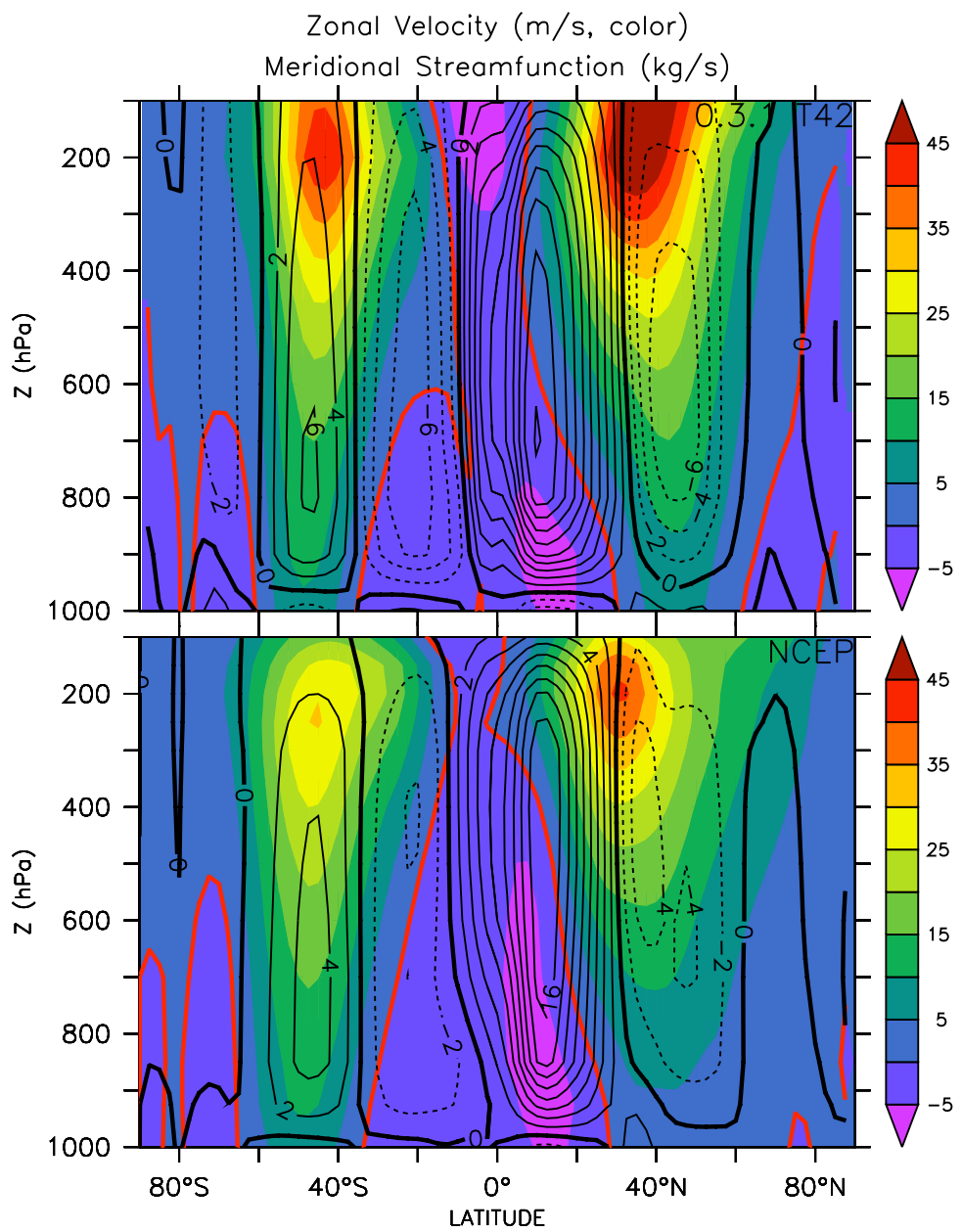


Figure 20: T42 Atmospheric Circulation DJF: Zonal mean zonal wind (color, zero contour line in red) and meridional mass streamfunction (black contour lines). Top model, bottom NCEP.

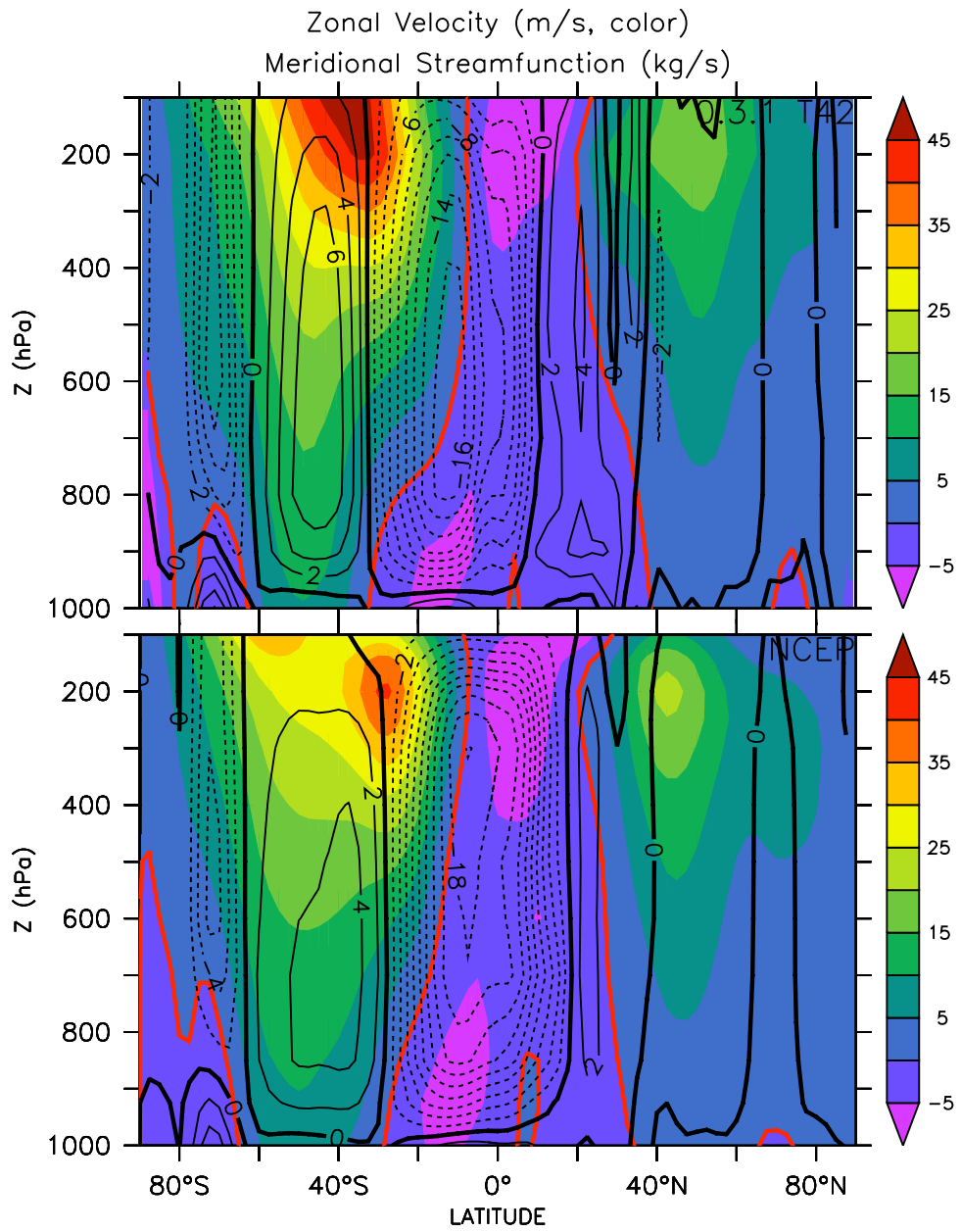


Figure 21: T42 JJA

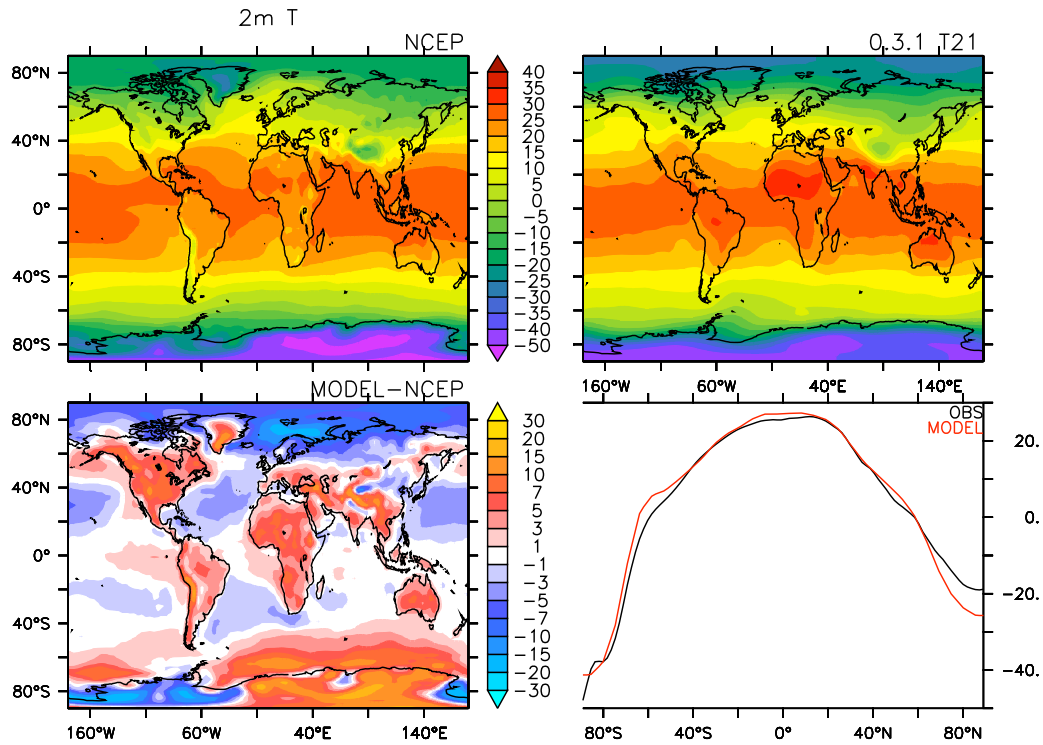


Figure 22: T21 Surface air temperature. Annual mean.

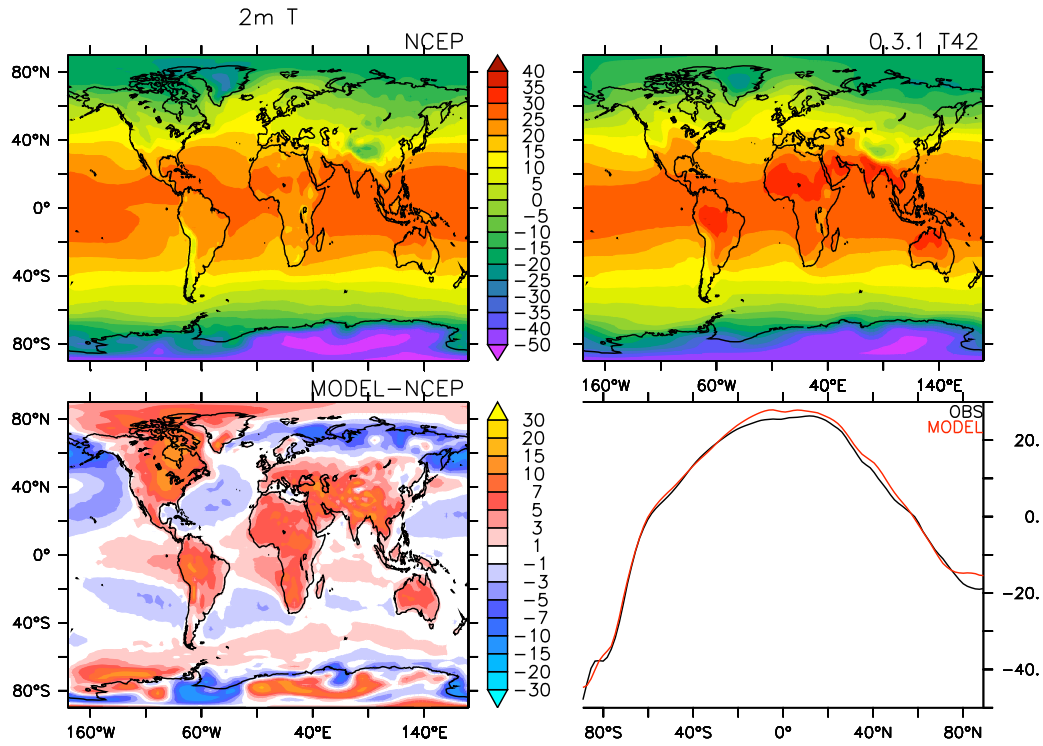


Figure 23: T42

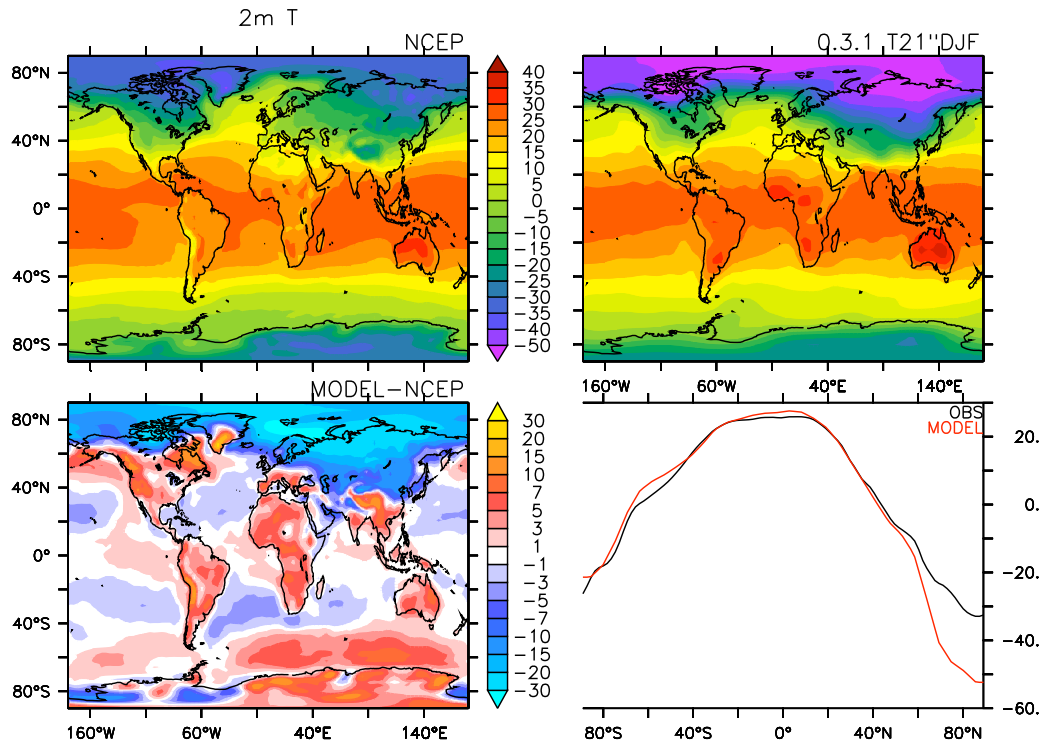


Figure 24: T21 Surface air temperature DJF

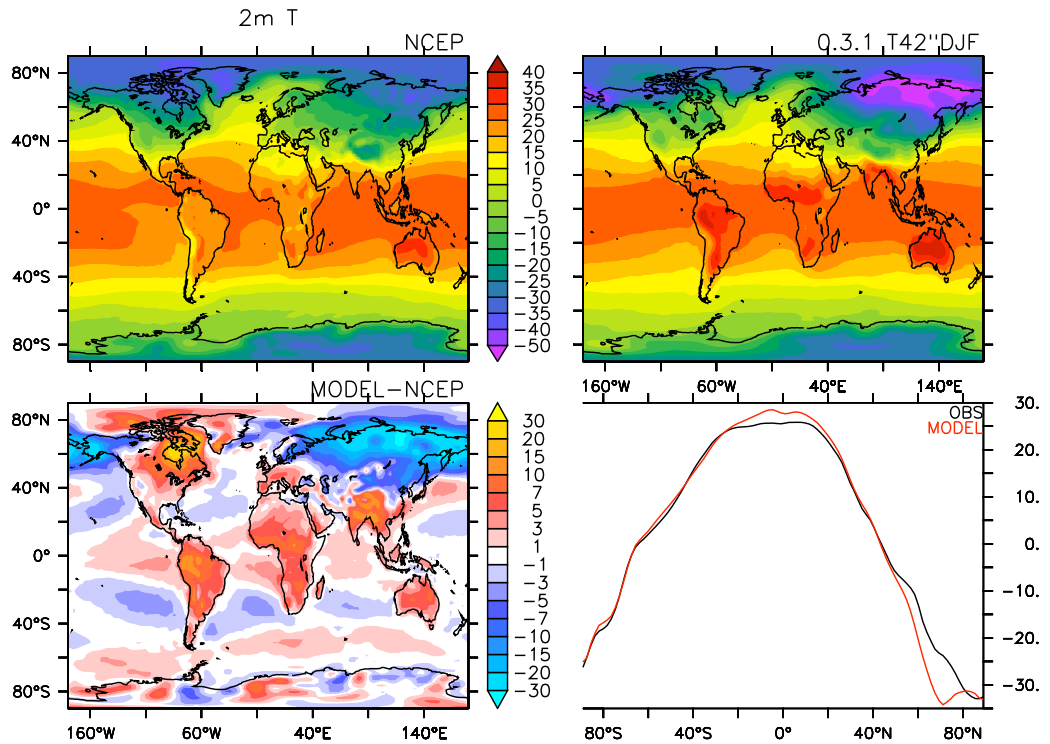


Figure 25: T42

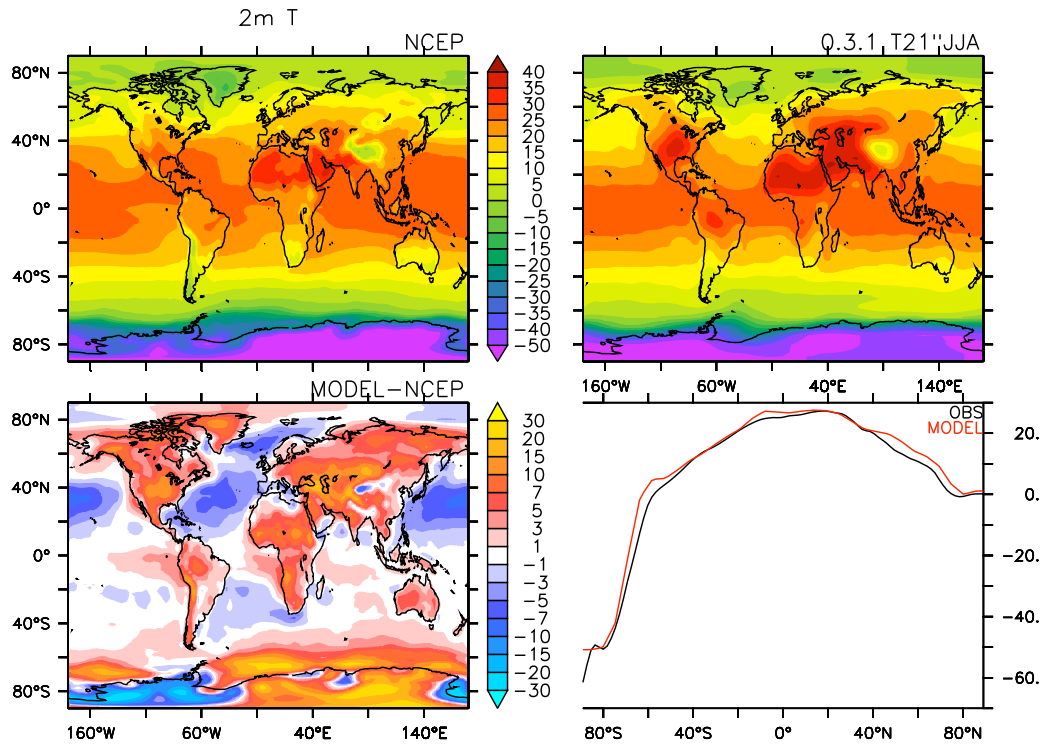


Figure 26: T21 Surface air temperature JJA

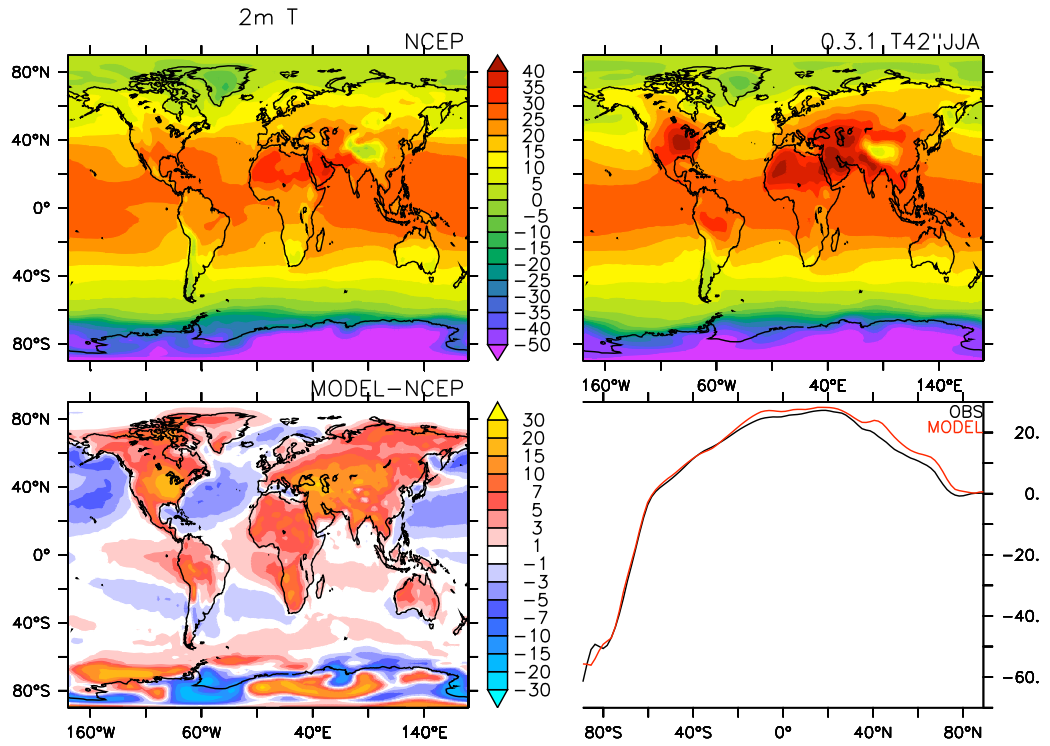


Figure 27: T42

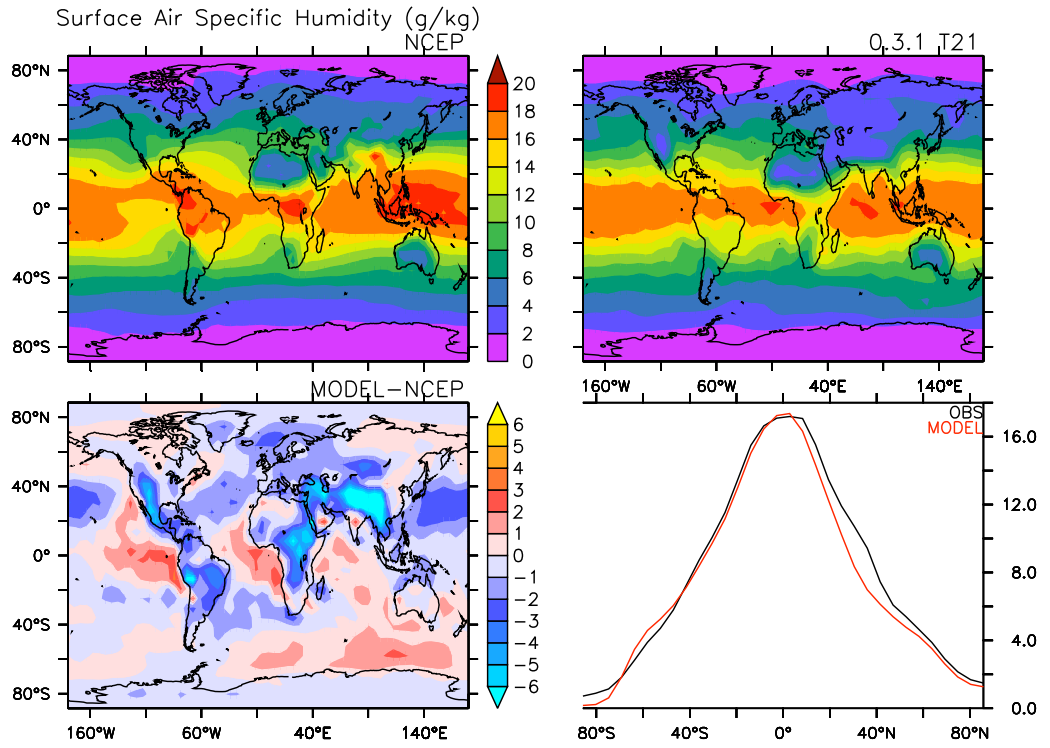


Figure 28: T21 Surface air specific humidity. Annual mean.

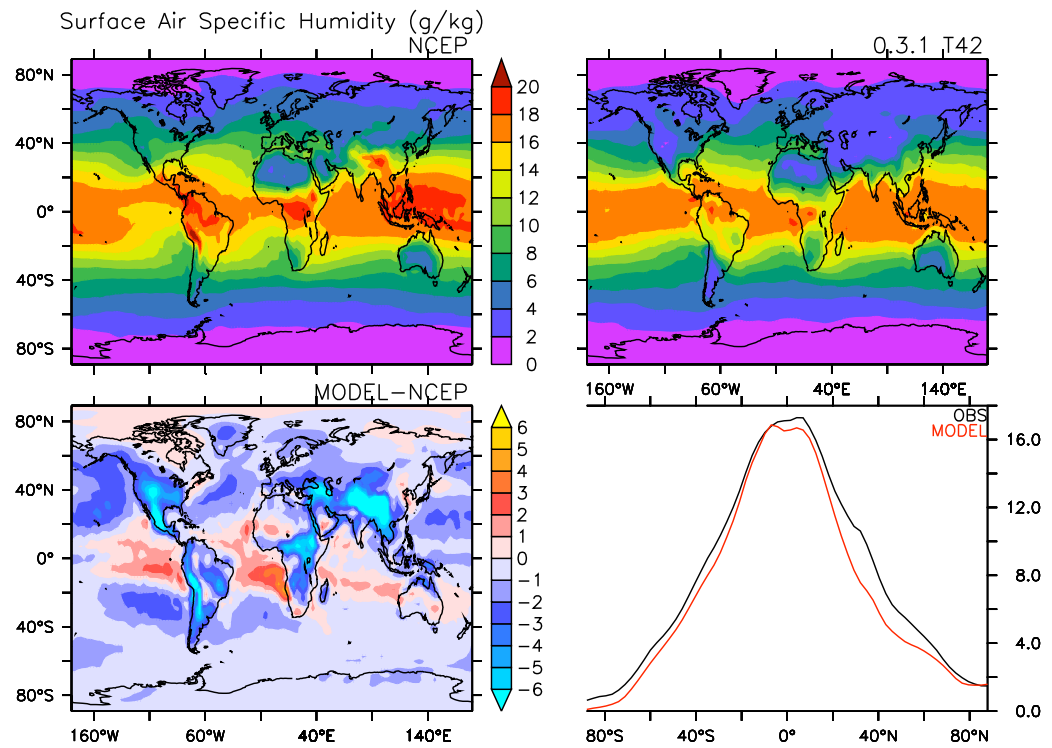


Figure 29: T42

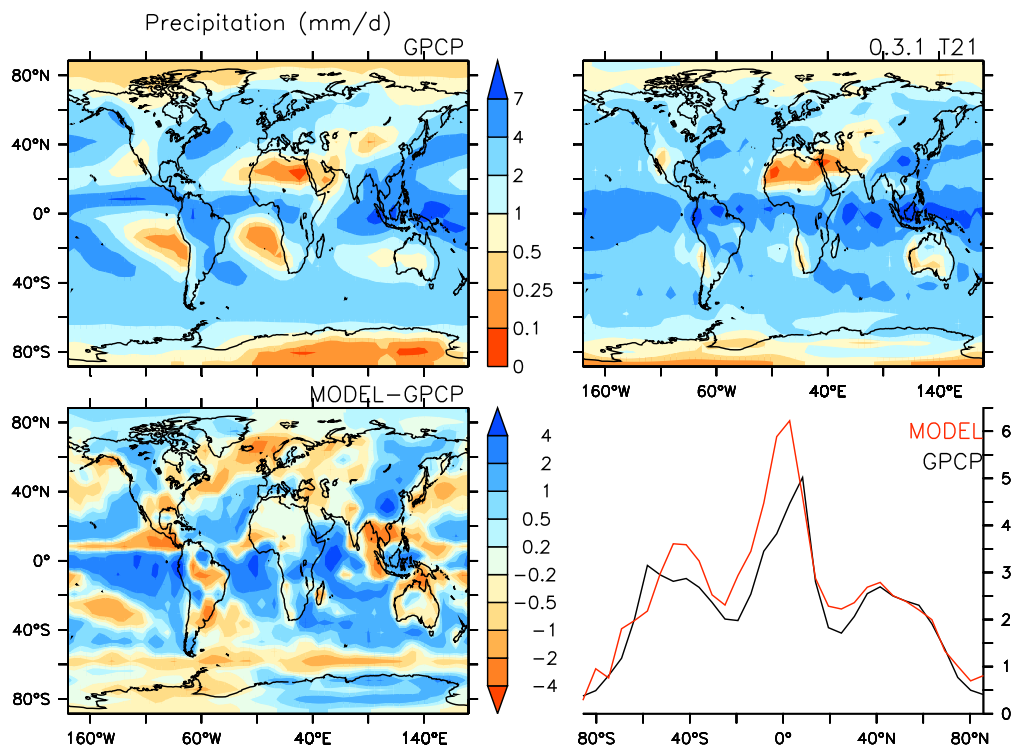


Figure 30: T21 Precip annual mean

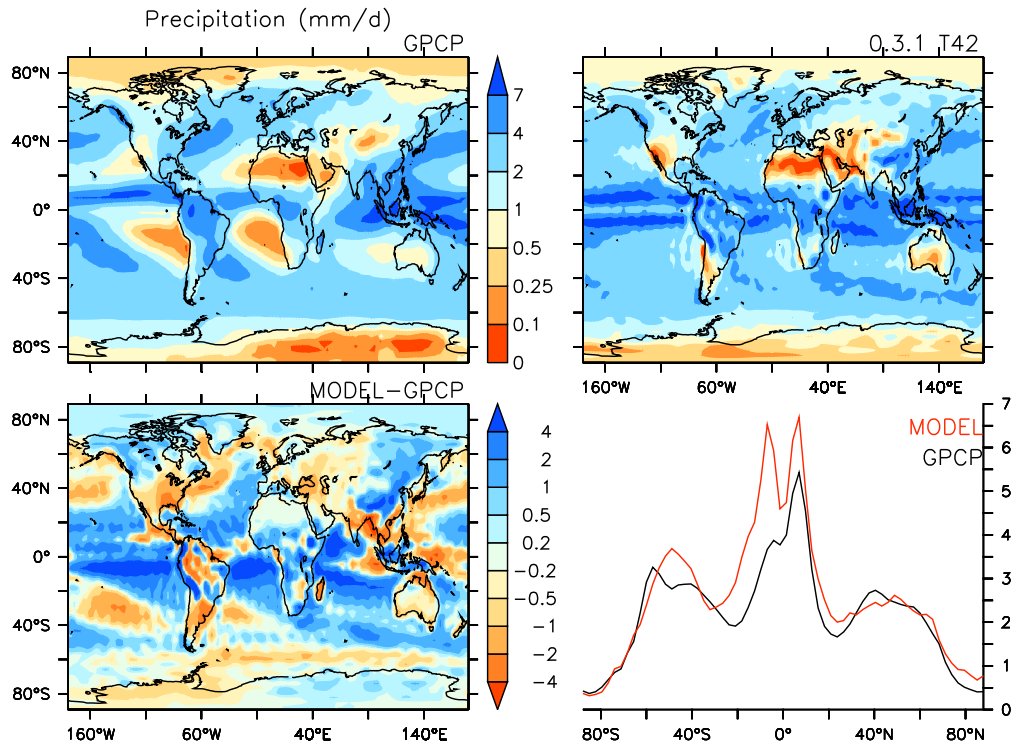


Figure 31: T42 Annual mean.

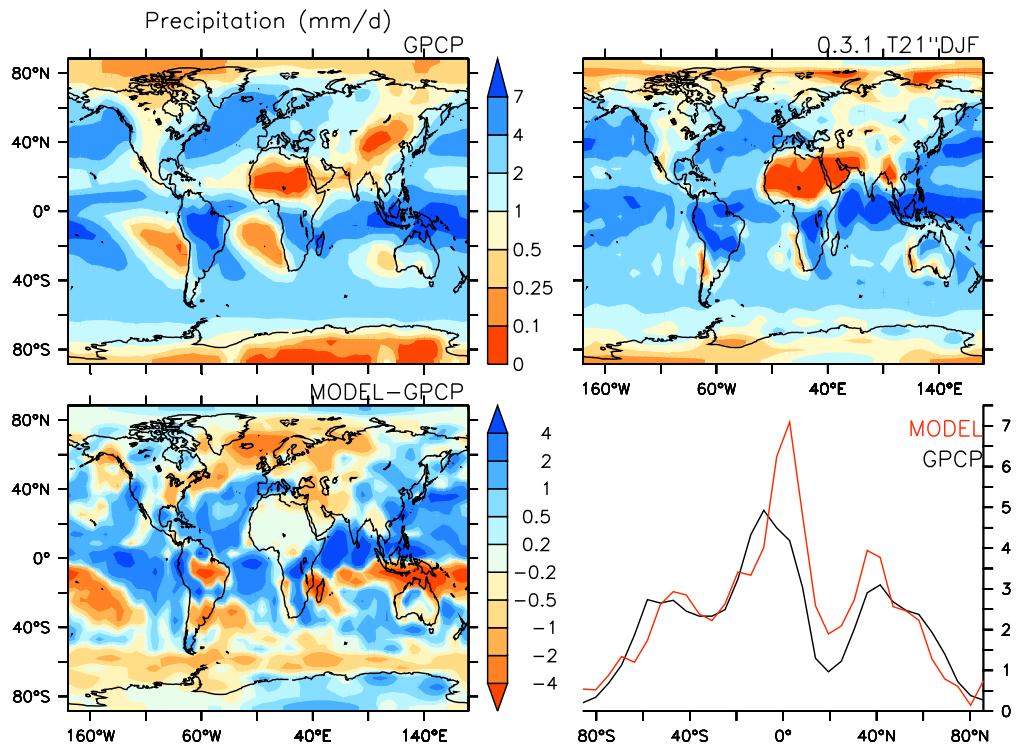


Figure 32: T21 DJF Precipitation

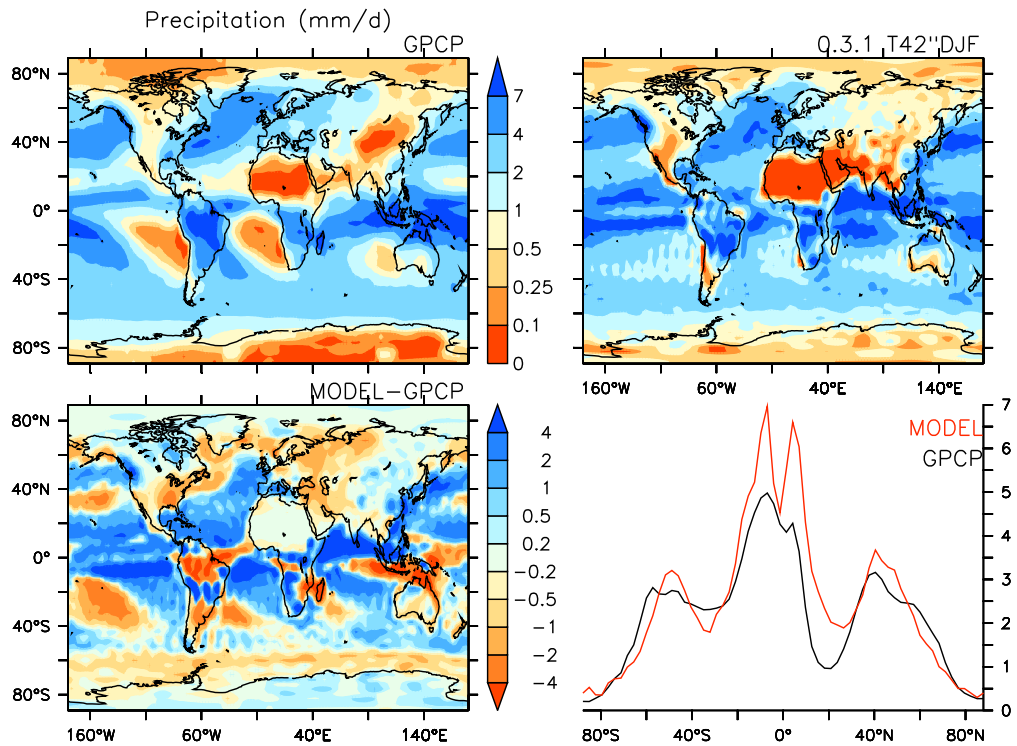


Figure 33: T42 Precipitation

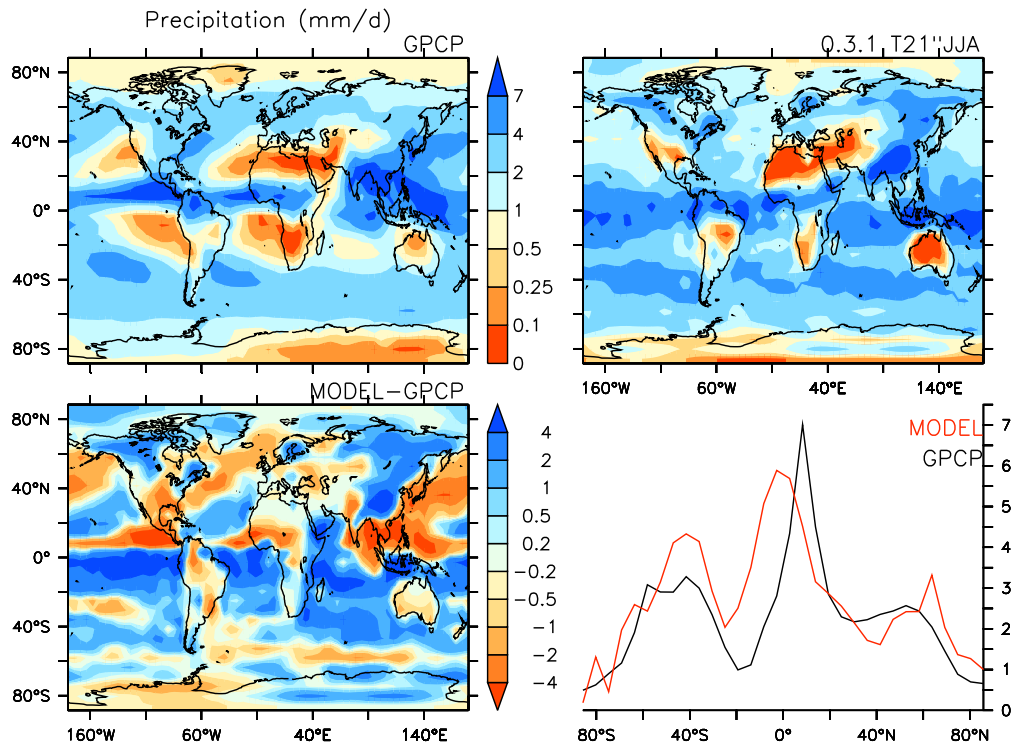


Figure 34: T21 JJA Precip.

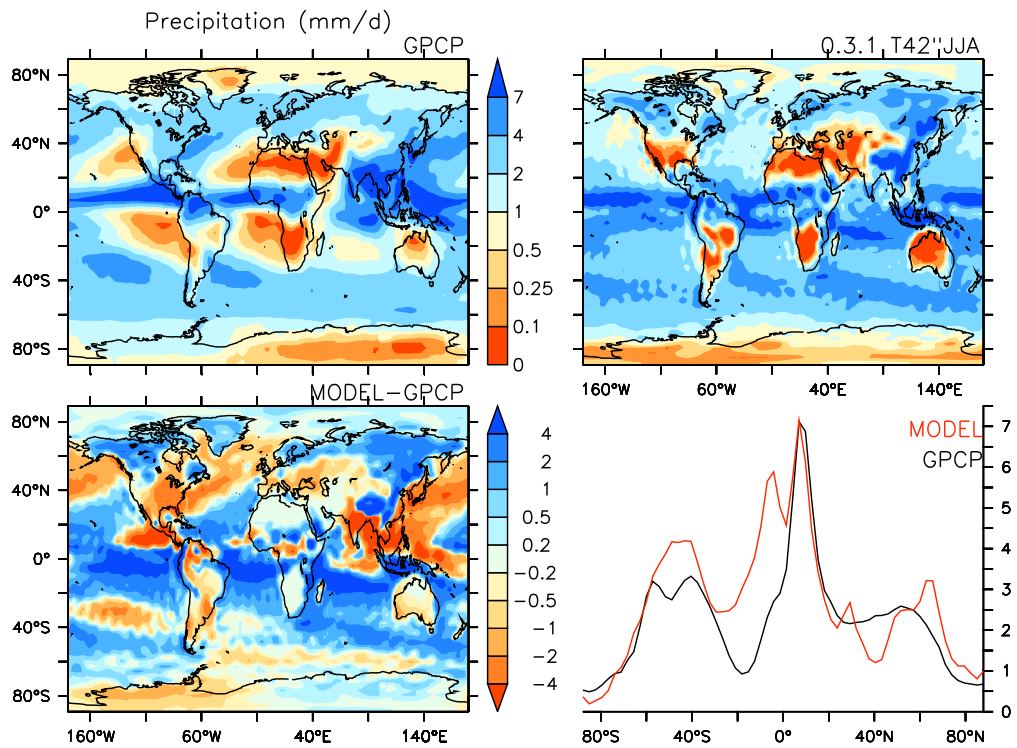


Figure 35: T42 JJA Precipitation.

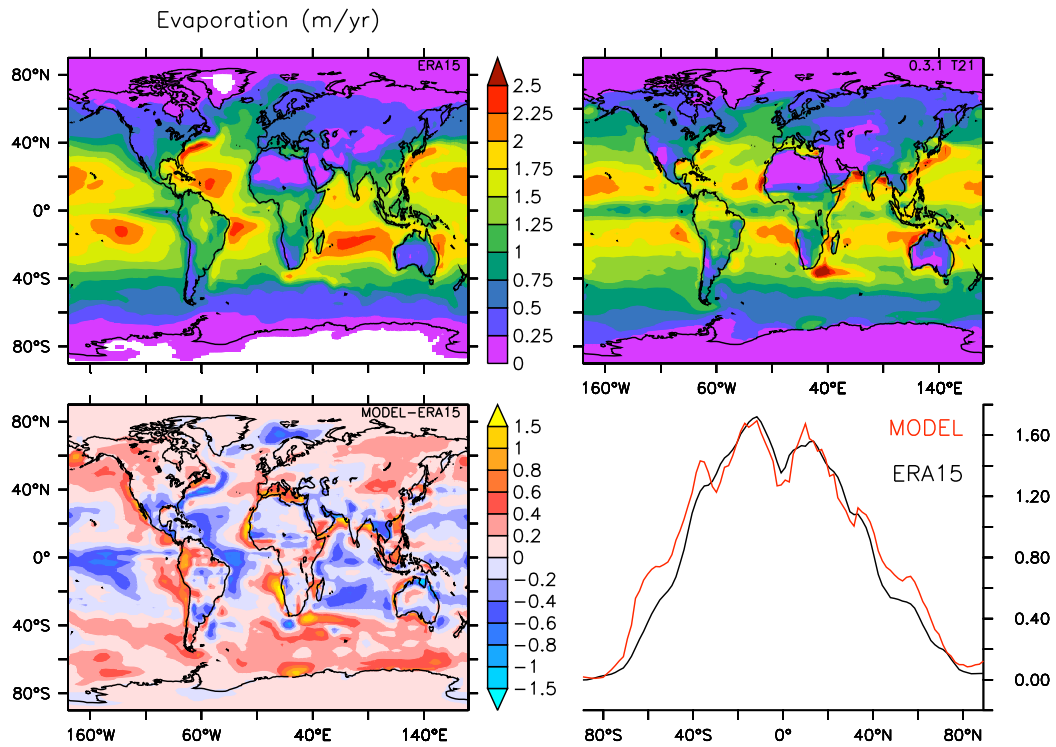


Figure 36 T21 Evaporation.

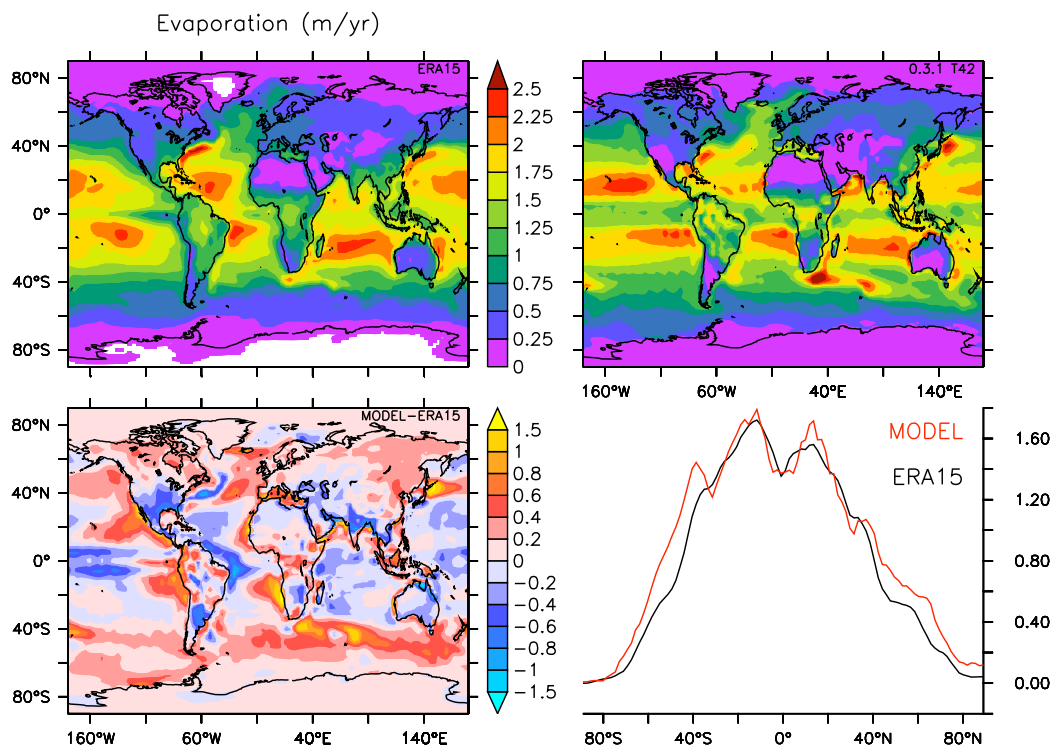


Figure 37 T42 Evaporation

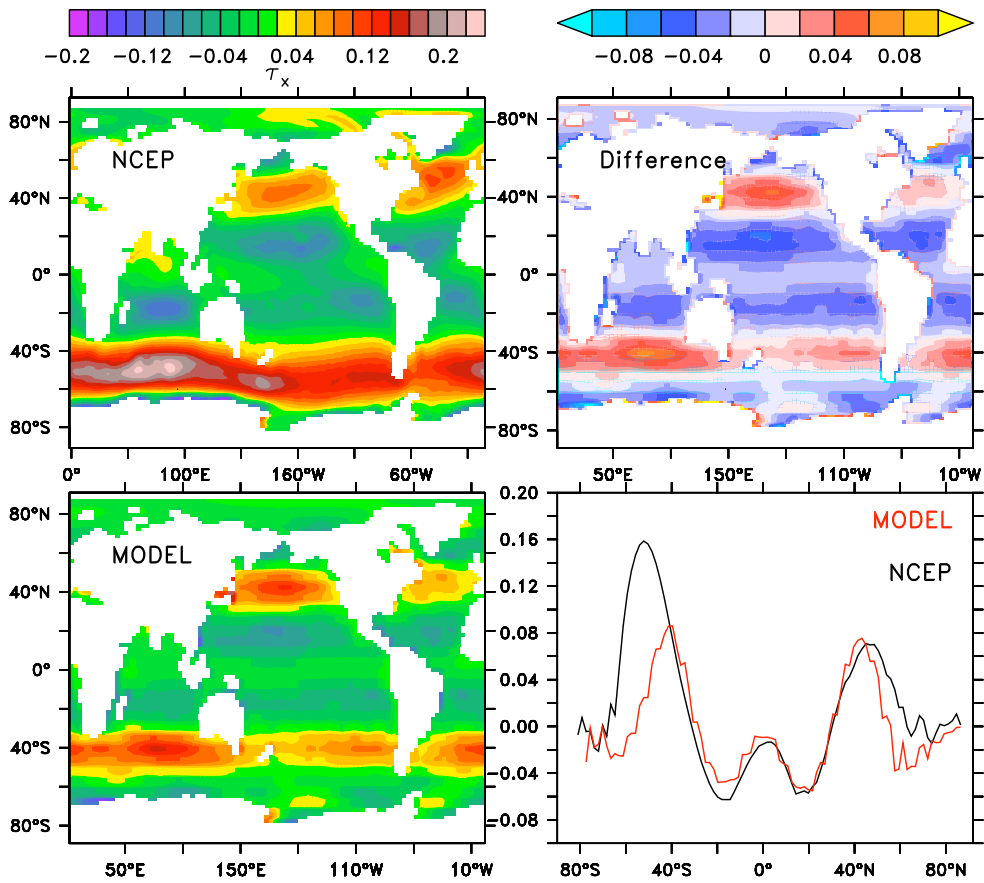


Figure 38: T21 Zonal windstress.

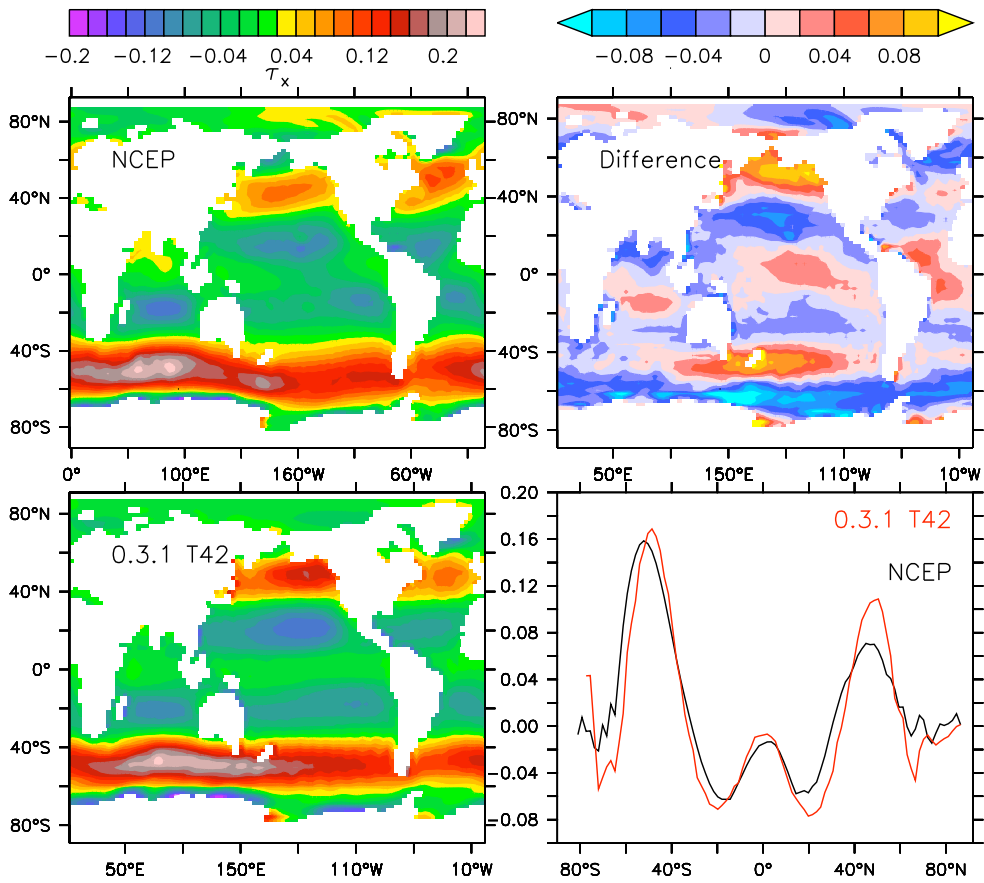


Figure 39: T42

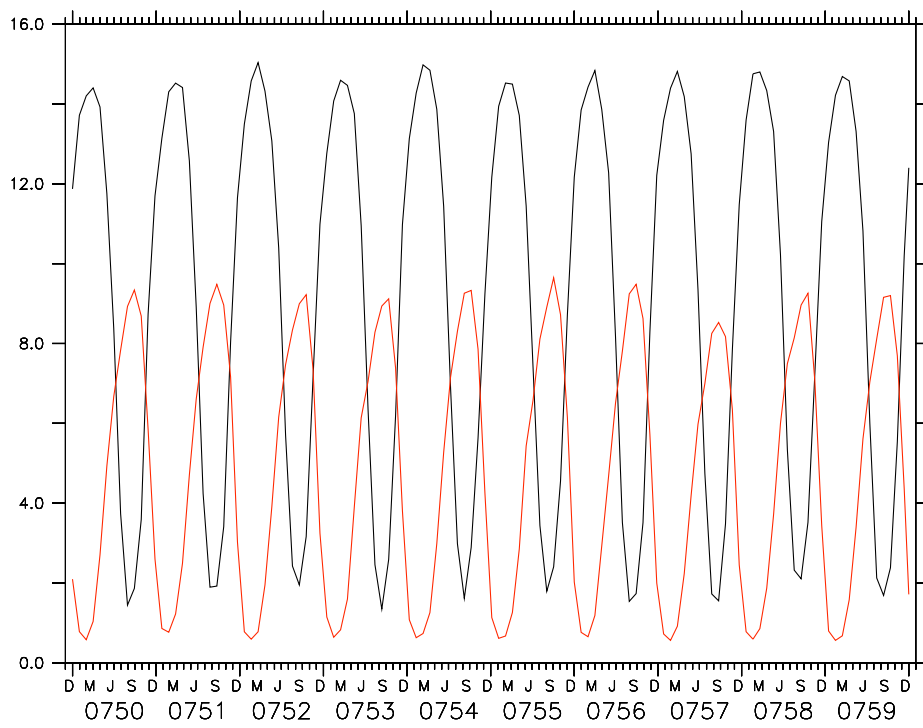


Figure 40: T21 Northern (black) and southern (red) hemisphere sea ice area (10^{12} m 2). Observations for southern hemisphere are 2(summer)-14(winter).

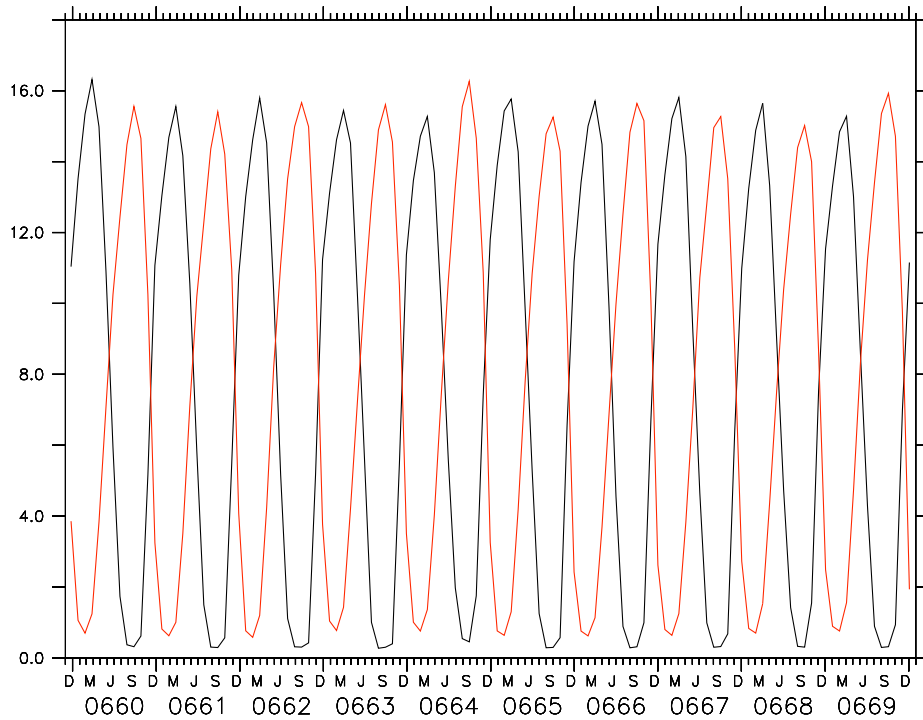


Figure 41: T42 Northern (black) and southern (red) hemisphere sea ice area (10^{12} m 2).

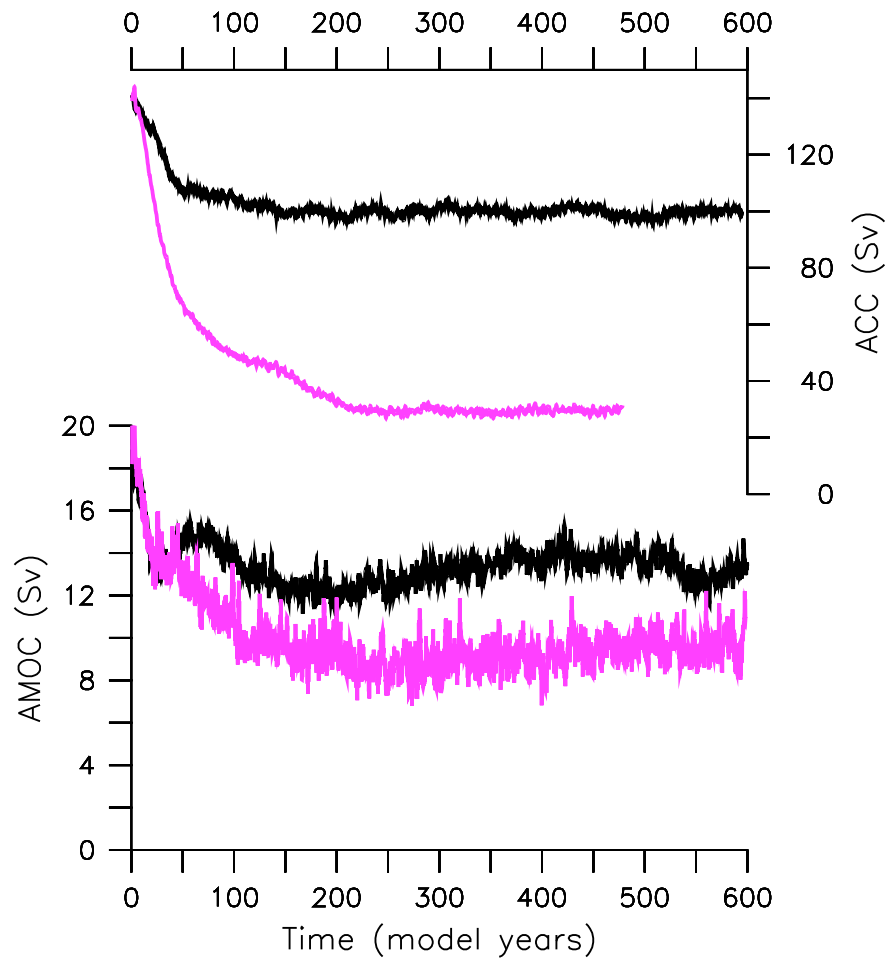


Figure 42: Ocean circulation indices. Top: Antarctic Circumpolar Current (ACC). Bottom: Annual mean Atlantic Meridional Overturning Circulation (AMOC) at 25N. T21 (purple), T42 (black). Observational estimates are ACC \sim 130 Sv and AMOC \sim 16 Sv.

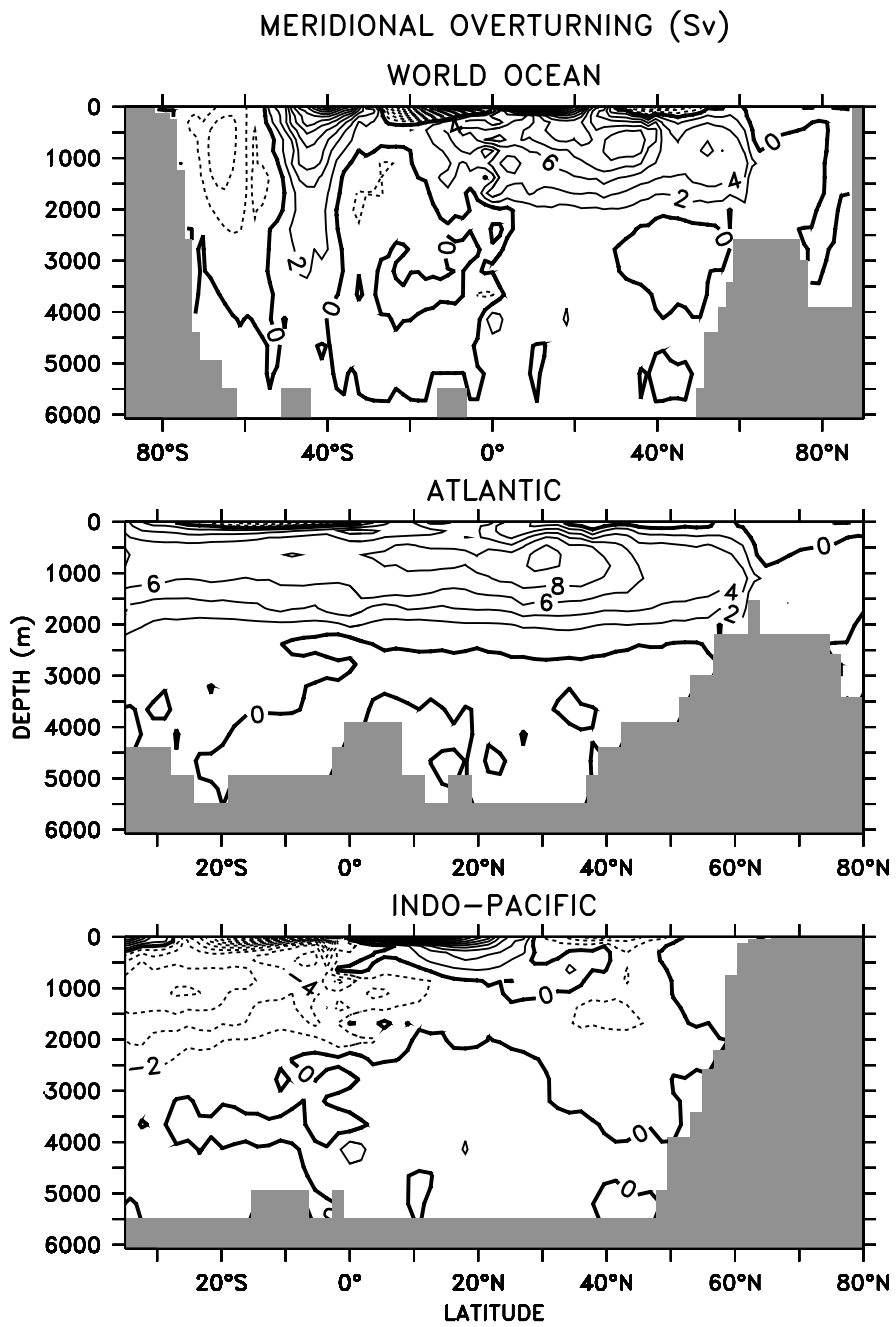


Figure 43: T21. Ocean meridional overturning circulation (Sv).

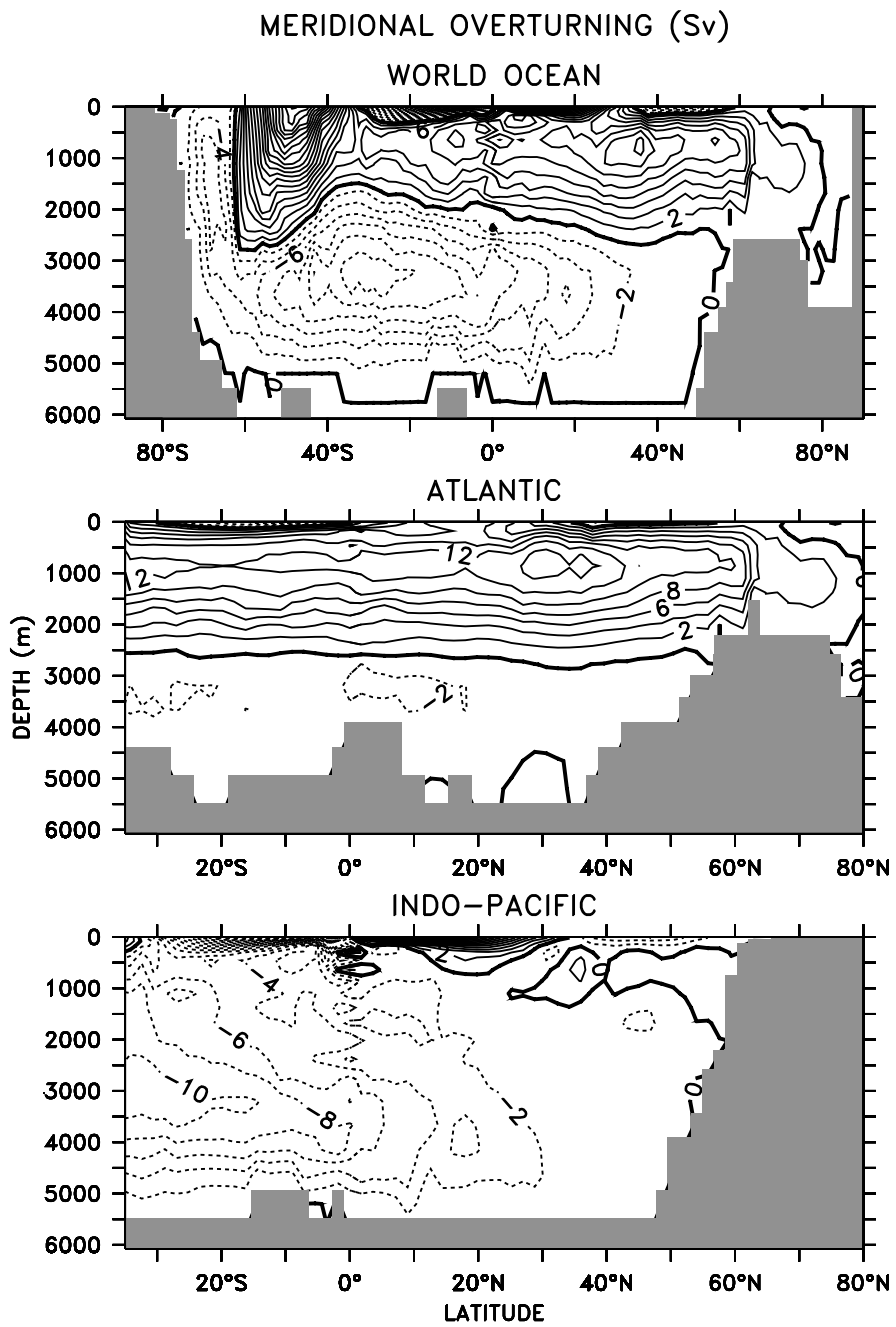


Figure 44: T42 MOC.

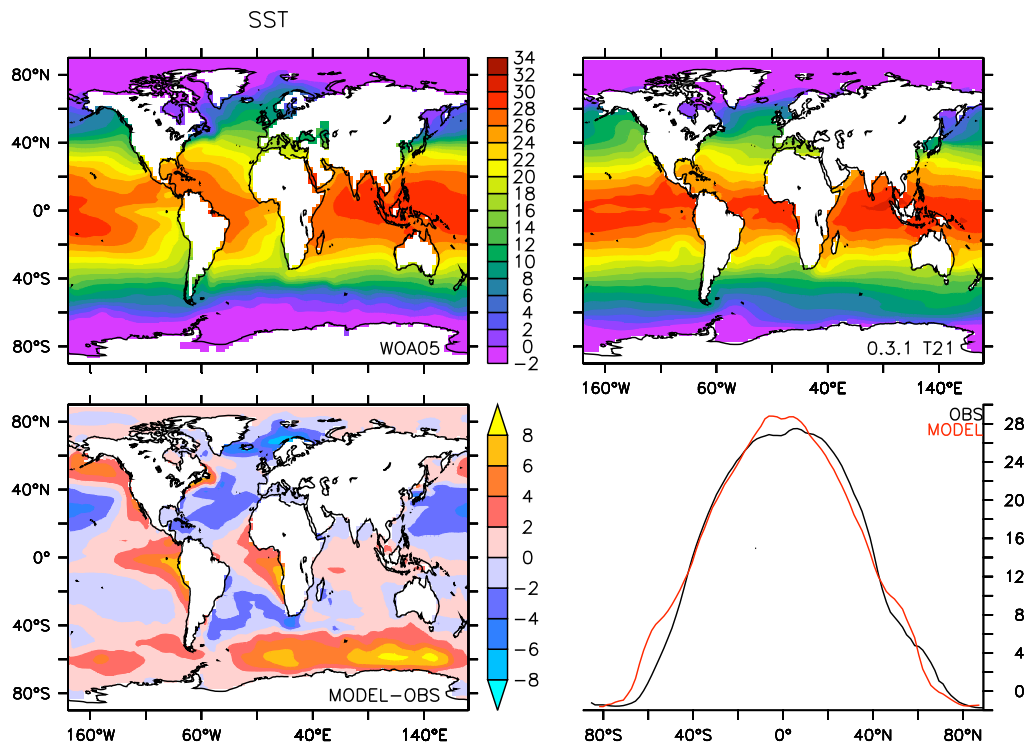


Figure 45: T21: SST

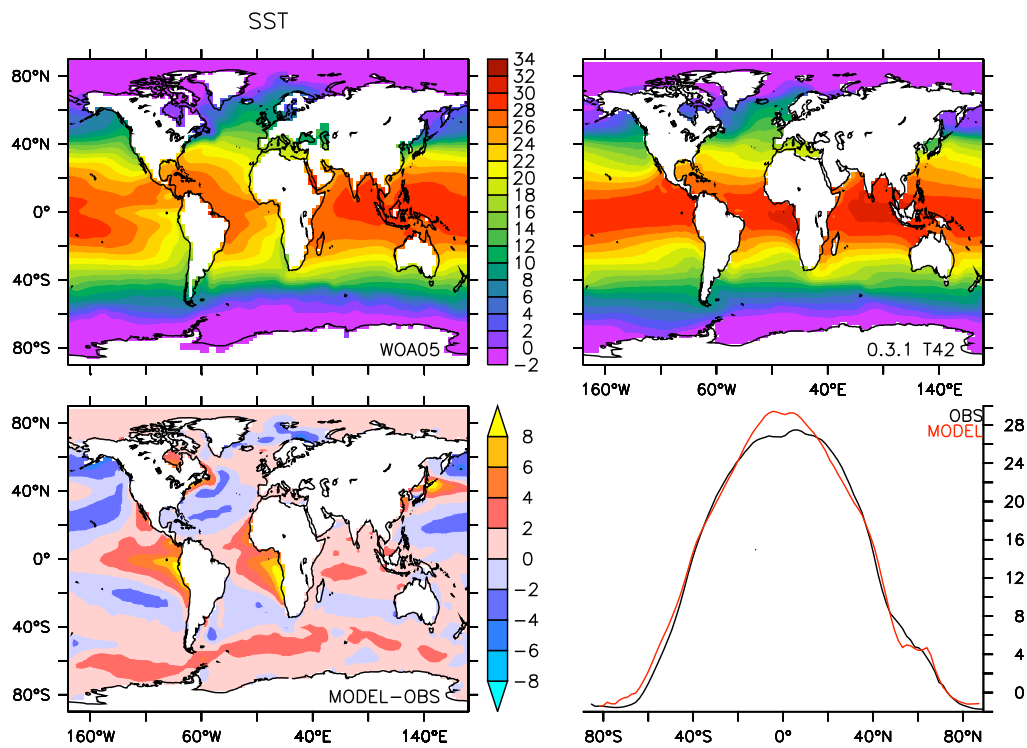


Figure 46: T42

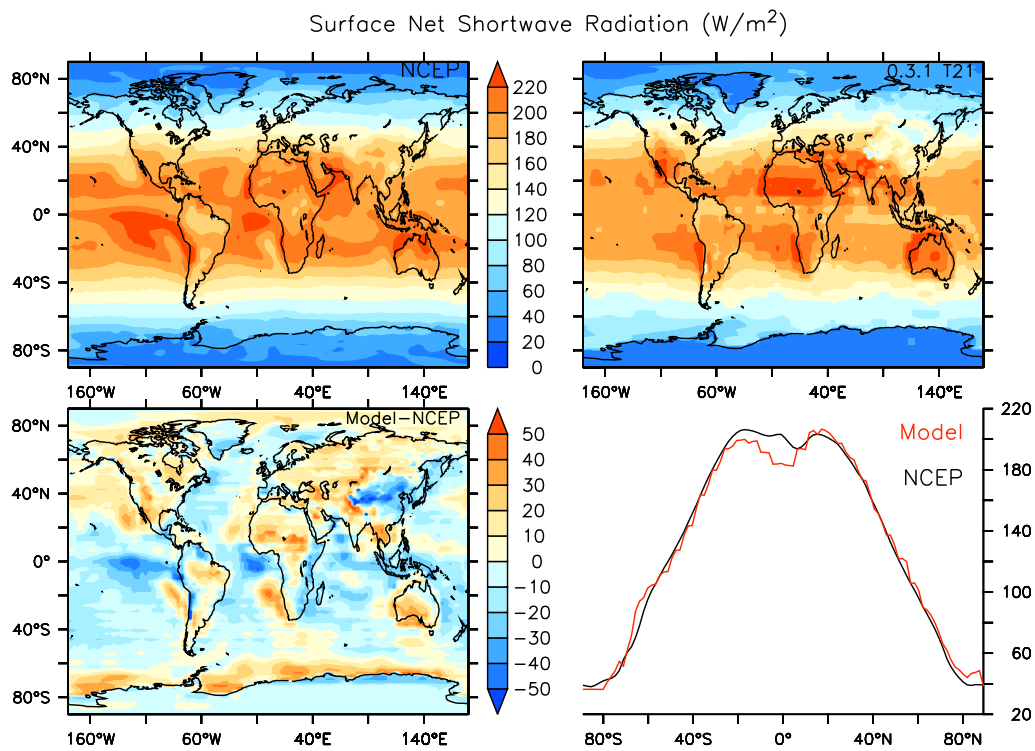


Figure 47: T21 SSW

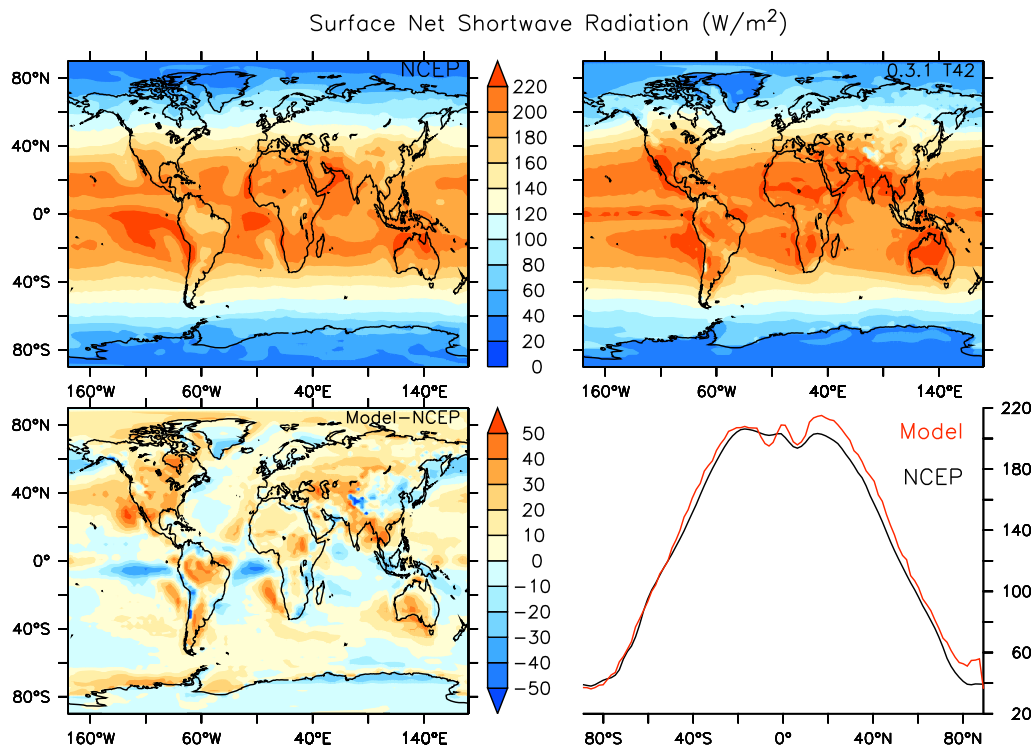


Figure 48: T42

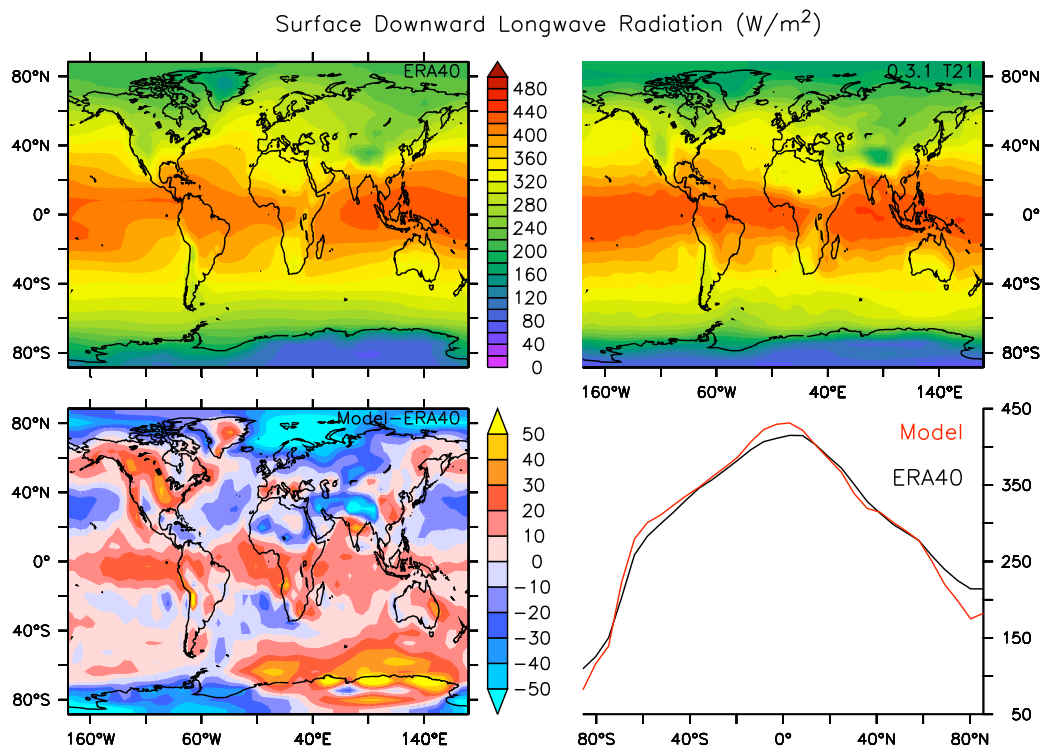


Figure 49: T21 STRD.

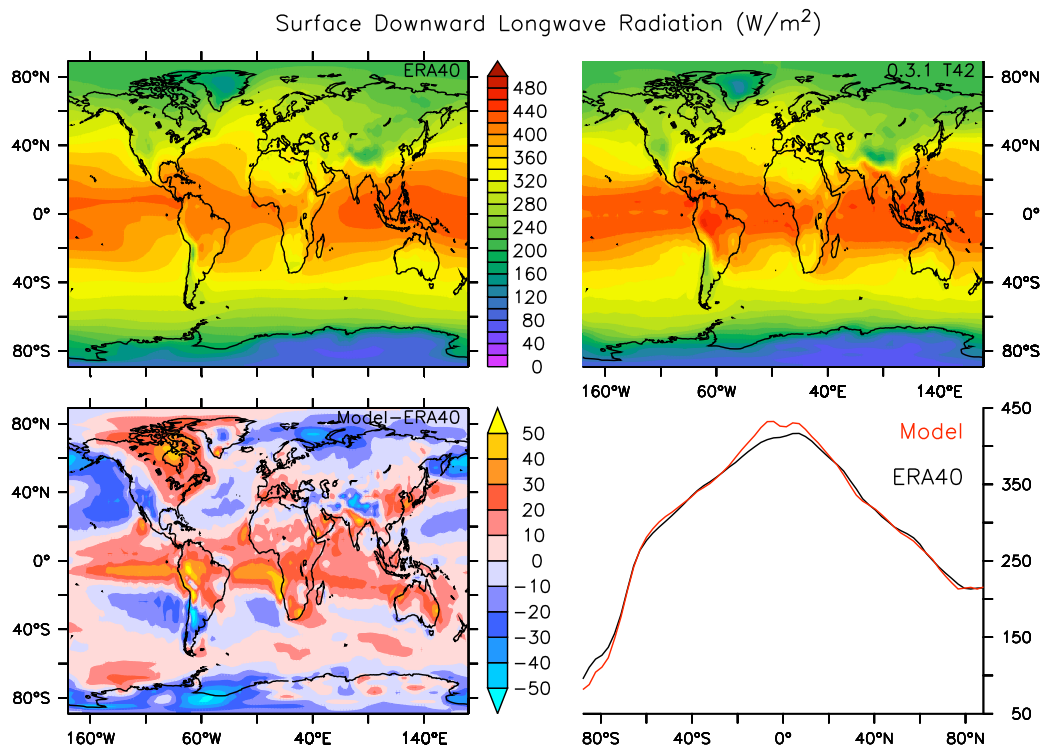


Figure 50: T42 STRD

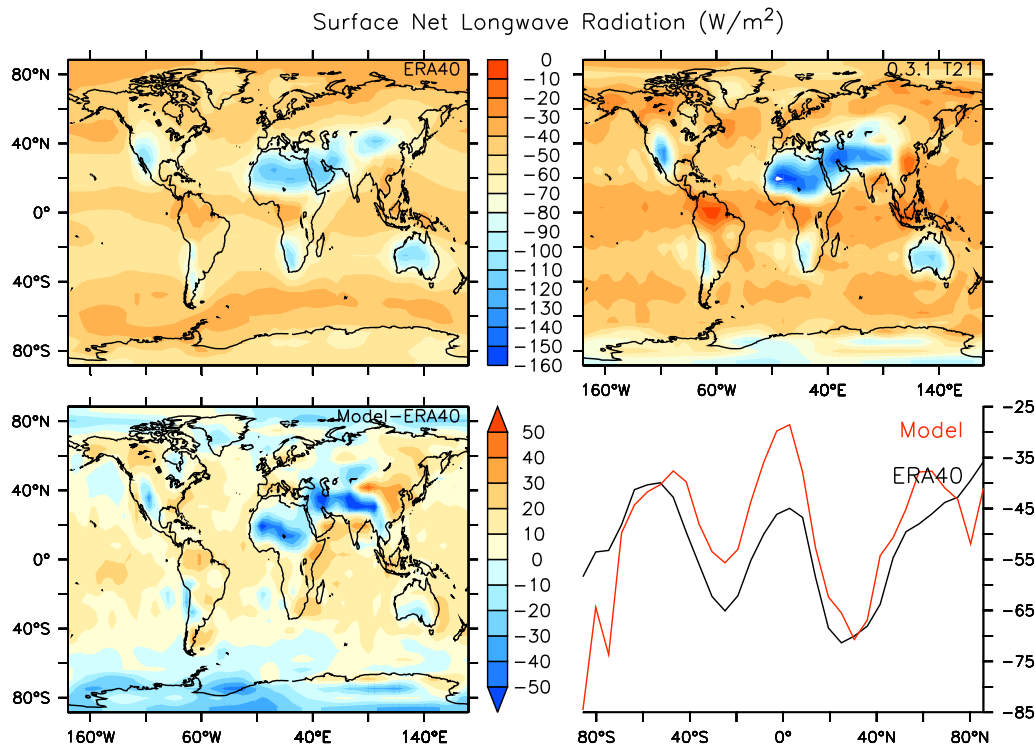


Figure 51: T21 SLW

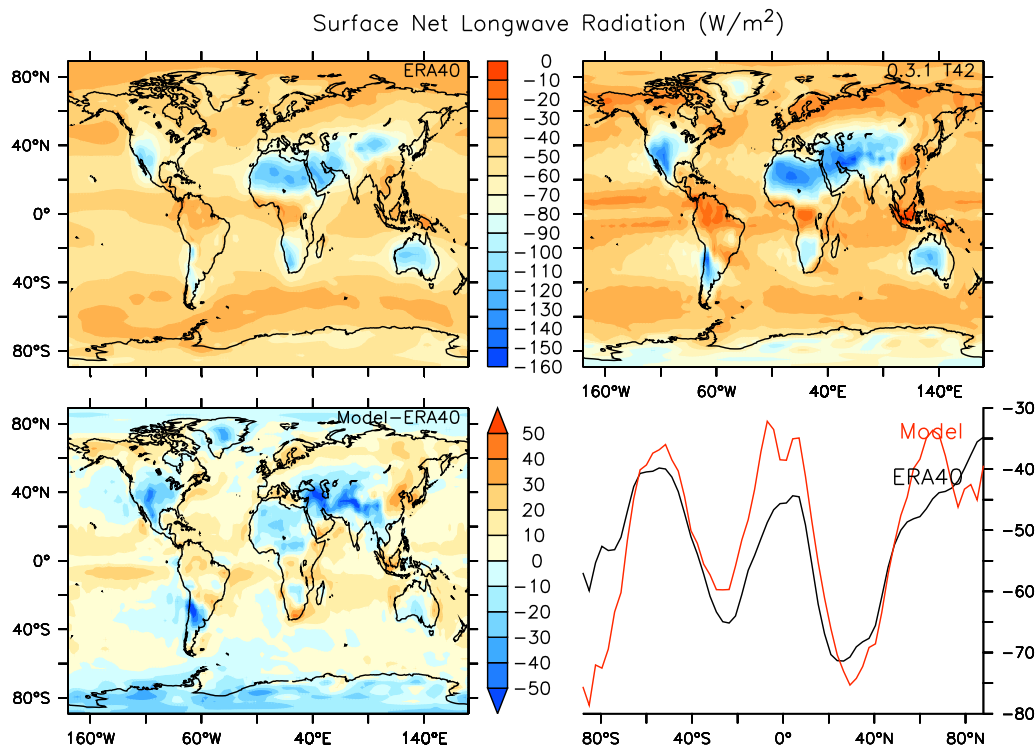


Figure 52: T42

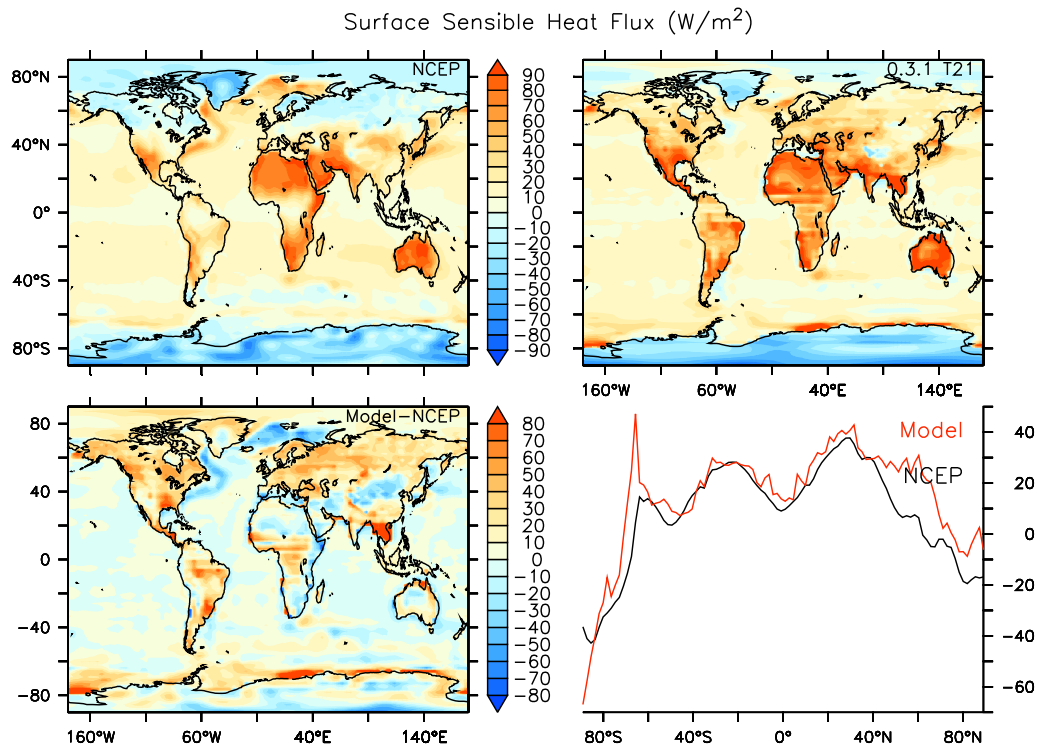


Figure 53: T21 SSH

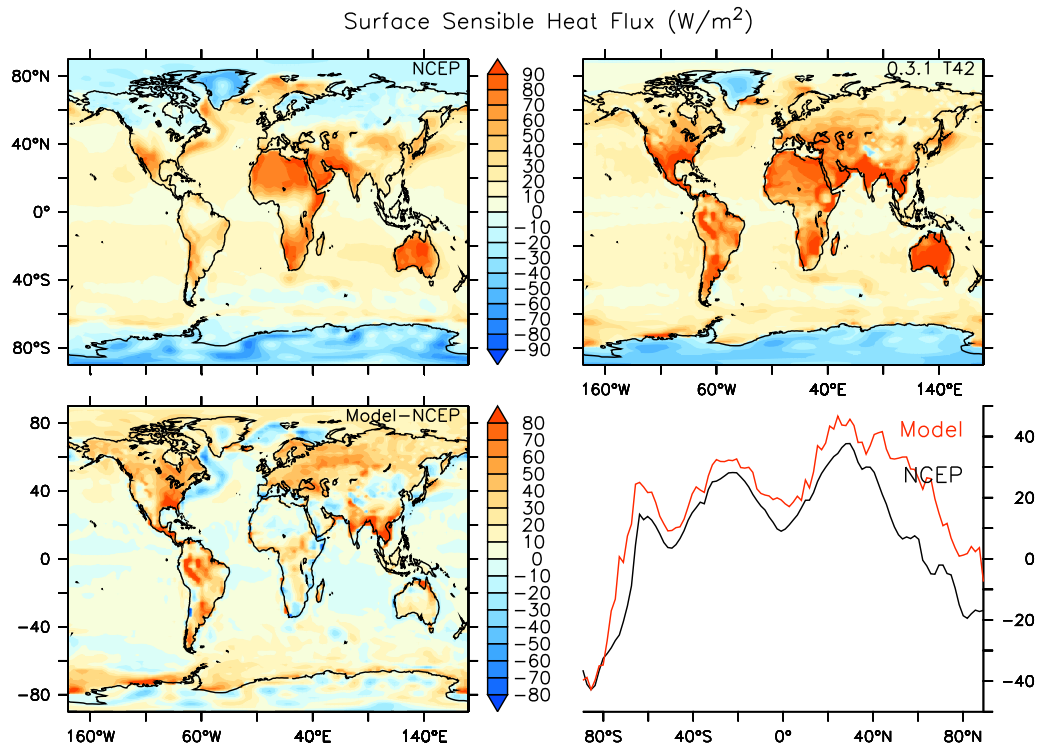


Figure 54: T42

REFERENCES

- Bryan, F. O., G. Danabasoglu, N. Nakashiki, Y. Yoshida, D. H. Kim, J. Tsutsui, and S. C. Doney (2006), Response of the North Atlantic thermohaline circulation and ventilation to increasing carbon dioxide in CCSM3, *J. Clim.*, 19(11), 2382-2397.
- Farneti, R., and G. K. Vallis (2009), An Intermediate Complexity Climate Model (ICCMp1) based on the GFDL flexible modelling system, *Geosci. Model Dev.*, 2(2), 73-88.
- Fraedrich, K., H. Jansen, E. Kirk, U. Luksch, and F. Lunkeit (2005a), The Planet Simulator: Towards a user friendly model, *Meteorologische Zeitschrift*, 14(3), 299-304, Doi 10.1127/0941-2948/2005/0043.
- Fraedrich, K., E. Kirk, U. Luksch, and F. Lunkeit (2005b), The portable university model of the atmosphere (PUMA): Storm track dynamics and low-frequency variability, *Meteorologische Zeitschrift*, 14(6), 735-745, Doi 10.1127/0941-2948/2005/0074.
- Jones, P. W. (1999), First- and second-order conservative remapping schemes for grids in spherical coordinates, *Monthly Weather Review*, 127(9), 2204-2210.
- Lunkeit, F., M. Bottinger, K. Fraedrich, E. Jansen, E. Kirk, A. Kleidon, and U. Luksch (2007), Planet Simulator Reference Manual Version 15.0.
- Peixoto, J. P., and A. H. Oort (1992), *Physics of Climate*, 520 pp., Springer, New York.
- Sasamori, T. (1968), The radiative cooling calculation for application to general circulation experiments, *J. Appl. Met.*, 7, 721-729.
- Schmittner, A., A. Oschlies, H. D. Matthews, and E. D. Galbraith (2008), Future changes in climate, ocean circulation, ecosystems and biogeochemical cycling simulated for a business-as-usual CO₂ emission scenario until year 4000 AD, *Glob. Biogeochem. Cycles*, 22, GB1013, doi:10.1029/2007GB002953: doi:10.1029/2007GB002953.
- Trenberth, K. E., J. T. Fasullo, and J. Kiehl (2009), Earth's Global Energy Budget, *B Am Meteorol Soc*, 90(3), 311-+.
- Weaver, A. J., M. Eby, E. C. Wiebe, C. M. Bitz, P. B. Duffy, T. L. Ewen, A. F. Fanning, M. M. Holland, A. MacFadyen, H. D. Matthews, K. J. Meissner, O. Saenko, A. Schmittner, H. X. Wang, and M. Yoshimori (2001), The UVic Earth System Climate Model: Model description, climatology, and applications to past, present and future climates, *Atmos.-Ocean*, 39(4), 361-428.